Context sensitivity of surface urban heat island at the local and regional scales

Yunfei Li[a,b,*], Bin Zhou[a,c], Manon Glockmann[a,b], Jürgen P. Kropp[a,b], Diego Rybski[a,d,e]

[a] *Potsdam Institute for Climate Impact Research – PIK, Member of Leibniz Association, P.O. Box 60 12 03, Potsdam 14412, Germany*
[b] *University of Potsdam, Institute for Environmental Science and Geography, Am Neuen Palais 10, 14469 Potsdam, Germany*
[c] *Ben-Gurion University of the Negev, Department of Geography and Environmental Development, P.O. Box 653, Be'er Sheva, Israel*
[d] *University of California Berkeley, Department of Environmental Science, Policy and Management, 130 Mulford Hall #3114, Berkeley, CA 94720, USA*
[e] *Complexity Science Hub Vienna, Josefstädterstrasse 39, A-1090 Vienna, Austria*

Abstract

In this study we analysed the multi-annual (2002-2011) average summer surface urban heat island (SUHI) intensity of the 5,000 largest urban clusters in Europe. We investigated its relationship with a proposed Gravitational Urban Morphology (GUM) index that can capture the local context sensitivity of SUHI. The GUM index was found to be an effective predictor of SUHI intensity. Together with other urban factors we built different multivariate linear regression models and a climate space based geographically weighted regression (GWR) model that can better predict SUHI intensity. As the GWR model captures the variation of influence from different urban factors on SUHI, it considerably outperformed linear models in predicting SUHI intensity in terms of R^2 and other statistical criteria. By investigating the variation of GWR coefficients against background climate factors, we further built a nonlinear regression model that takes into account the sensitivity of SUHI to regional climate context. The nonlinear model showed comparable performance to that of

the GWR model and it prevailed against all the linear models. Our work underlines the potential of SUHI reduction through optimising urban morphology, as well as the importance of integrating future urbanisation and climate change into the implementation of urban heat mitigation strategies.
Keywords: urban form;, surface urban heat island;, climate context;, geographically weighted regression

---

Highlights:

- A Gravitational Urban Morphology (GUM) index that captures the local scale context sensitivity of SUHI was proposed.
- The GUM index can serve as an effective predictor of SUHI intensity.
- Climate space based GWR model outperformed linear models for SUHI assessment.
- A nonlinear model that captures the regional climate context sensitivity of SUHI performs well.

---

*Corresponding author.
Email address: yunfei.li@pik-potsdam.de (Yunfei Li)

Notations	
UHI	urban heat island
SUHI	surface urban heat island
GUM index /D	gravitational urban morphology index
GWR	geographically weighted regression
LST	land surface temperature
OLS	ordinary least squares
LCZ	local climate zone
LULC	land use/land cover
EVI	enhanced vegetation index
ΔT	surface urban heat island intensity, [°C]
A	urban area, [km^2]
$U_{\Delta Wat}$	water surface fraction difference between urban area and boundary area
$U_{\Delta Veg}$	EVI difference between urban area and boundary area
$U_{\Delta Ele}$	elevation difference between urban area and boundary area, [m]
B_{Ele}	average elevation of boundary area, [m]
B_{Win}	average summer wind speed of boundary area, [ms^{-1}]
B_{Pre}	average summer precipitation of boundary area, [mm]
B_{Tmx}	average summer maximum daily temperature of boundary area, [°C]
B_{Lat}	Latitude of the urban centroid

1. Introduction

The urban heat island (UHI) effect, which refers to the phenomenon that urban areas tend to experience higher temperatures than their rural surroundings, is one of the clearest examples of anthropogenic climate modification (Oke et al., 2017). The UHI effect has various impacts on the local environment and human health (Grimm et al., 2008). The most direct adverse impacts are heat-related health problems (Tan et al., 2010) and increased risk of heat morbidity and mortality (Gabriel and Endlicher, 2011; Krummenauer et al., 2019) during hot summer days, as in many cities the UHI effect exposes urban dwellers to extra heat stress.

There are several types of UHI according to the schemes used to measure them (Oke et al., 2017). Among them, the surface UHI (SUHI), measured by urban/non-urban radiative temperature differences derived usually from satellite land surface temperature (LST) data, has attracted considerable interest in recent years due to the advancement of remote sensing techniques, as well as its association with rapid urbanisation and global warming which draw increasing attention (Zhou et al., 2019a). The advantages (e.g. spatial/temporal resolution and coverage, data accessibility) of remote sensing data enable researchers to conduct spatially-explicit studies at various spatial and temporal scales (Deilami et al., 2018; Zhou et al., 2019a).

Case studies on small scales (e.g. raster pixel, block, and district level) usually try to explore spatial or temporal SUHI variations to examine statistically a wide range of factors (for example, share of vegetation and impervious surface, building density, etc.) and their

contributions to SUHI (Deilami et al., 2018; Li et al., 2018; Yang et al., 2019). Studies at this scale often take the LST as proxy of SUHI intensity and mainly use ordinary least squares (OLS) regression with one or more factors as predictors (Deilami et al., 2018). Recently, an increasing number of studies on the relationship between local climate zones (LCZs) and SUHI intensity (Demuzere et al., 2019; Geletič et al., 2019; Ochola et al., 2020) have been published with resort to the LCZ classification scheme proposed by Stewart and Oke (2012). Some researchers also try to link SUHI variations across time with the dynamic of land use/land cover (LULC) (Singh et al., 2017; Sultana and Satyanarayana, 2020).

However, due to fluxes and energy flows between different LULC types, the landscape heterogeneity also plays an important role (Li et al., 2017; Zhou et al., 2019b) and therefore the SUHI is context sensitive at the local scale (Song et al., 2014). It was found when taking the effects of neighbouring elements (e.g. grid cell or landscape patch) into account by using spatial regression models (Chun and Guldmann, 2018; Yin et al., 2018; Dai et al., 2018; Galletti et al., 2019; Guo et al., 2020) or geographically weighted regression (GWR) models (Buyantuyev and Wu, 2010; Li et al., 2010; Su et al., 2012; Szymanowski and Kryza, 2012; Deilami et al., 2018; Liu et al., 2019; Zhang et al., 2019), higher explanatory or predictive power can be obtained to model/assess the relationship between SUHI variations and the contributing factors. This implies that SUHI at the local scale is influenced by the proximity to and the spatial distribution of nearby warming/cooling factors, and this influence decays as the distance increases.

With this in mind, one could easily arrive at the presumption that when the city is considered as a whole, urban morphology (used in the narrow sense, refers mainly to geometric

form) could also have an impact on the city-scale SUHI effect, as urban morphology per se is the aggregated result of the spatial configuration/placement of the fine-scale urban elements. Although many studies (Deilami et al., 2018; Zhou et al., 2019a) have compared SUHI intensities of different cities and attempted to explore the influence of city-level factors (e.g. urban size and density) (Zhou et al., 2013; Li et al., 2017; Song et al., 2020) on SUHI, only a few efforts have been addressed regarding the influence of urban morphology on SUHI. The reasons may be twofold. On the one hand, cities are complex systems with high heterogeneity in various aspects, a less pronounced association between the urban morphology and SUHI intensity is more likely to be obscured by the noise. For example, "compact city" means denser land utilisation but probably also leads to less traffic emission (Wang et al., 2015), to which extent the influence from one of these two aspects prevails the other varies across cities. On the other hand, the difference in biophysical background may further dim the signal from inter-city statistics as the SUHI effect is also sensitive to the regional background climate (Peng et al., 2012; Zhao et al., 2014; Zhou et al., 2014; He, 2018; Manoli et al., 2019).

Regardless of the challenges, some previous investigations provided important insights on this topic. For example, Zhang et al. (2012) analysed the SUHI of 42 northeastern US urban areas within the same ecological context, and they found a linear relationship between SUHI intensity and an urban shape indicator calculated as logarithmic urban area/perimeter ratio. In order to reduce the noise from background climate, Liang et al. (2020) studied SUHI of 150 cities with a relatively uniform climate condition in the Jing-Jin-Ji region of China. Based on various regression models, urban form indicators like fractal dimension, contiguity,

elongation have been found to have a stronger positive contribution to the summer daytime SUHI, whereas for SUHI during nights or other seasons, their contributions vary both quantitatively and qualitatively. Some studies also explored qualitatively the climate sensitivity of the relationship between SUHI and urban morphology. For instance, from the statistics based on the 5,000 largest urban clusters in Europe, Zhou et al. (2017) found that a compact urban form featured with large box-counting fractal dimension and small anisometry tends to increase the summer SUHI intensity whilst the influence varies regionally. In a more recent work, Liu et al. (2021b) examined the relationships between different urban form metrics and SUHI intensity based on 1288 urban clusters in China and they found these relationships vary against the climate zones.

These findings advance our understanding of the influence of urban morphology on SUHI as well as its sensitivity to the climate context. However, the quantitative understanding of this sensitivity, which is important for fast SUHI assessment across climate regions, is still lacking. Moreover, urban morphology indicators used in previous studies focus mainly on 2D morphology of the urban clusters or their component elements, while the spatial pattern of the intra-city heterogeneity in density, which are key to capture the context sensitivity of SUHI at the local scale, are largely underrepresented.

Recently, based on numerical climate simulations with generated 3D urban structure data (Li et al., 2021), Li et al. (2020) proposed a 3D urban morphology indicator that was found to be an effective quantitative indicator linking urban form and canopy UHI intensity. Although physical processes behind the SHUI effect and the canopy UHI effect are different (Oke et al., 2017; Peng et al., 2012), the underlying assumption may still apply

in both cases, i.e. individual urban cells exert a warming/cooling effect on each other which decays with distance. This assumption is consistent with the context sensitivity of SUHI at the local scale. Therefore, whether a similar indicator also applies for SUHI is worth an exploration. As in (Li et al., 2020) the urban morphology indicator was calculated resembling the gravitational force, hereafter we name it *Gravitational Urban Morphology* index and GUM index in short.

In this work we extract the 5,000 largest urban clusters in Europe and calculate their SUHI intensities as well as GUM index similar to Li et al. (2020) and analyse the correlations between both. Further, various regression models are built by taking several city-level variables as predictors, such as urban size, urban-rural difference in vegetation, and water surface share. We explore quantitatively the context sensitivity of SUHI to the regional climate with resort to climate space based GWR model. We explore quantitatively the background climates governed influences of urban factors on SUHI and illustrate how background climate factors can be integrated into a nonlinear model that outperforms linear ones.

2. Data and methods

2.1. Data

The binary urban/non-urban Urban Morphological Zones 2006 (UMZ2006) data-set at 250m resolution from the European Environment Agency (EEA) was used to delineate the urban/non-urban area. It was created from CORINE Land Cover data of the year 2006 (CLC2006) following the reclassification method as described in (Simon et al., 2010).

UMZ2006 covers 38 European Environmental Agency member states and cooperating countries except Greece.

The LST data set from the Moderate Resolution Imaging Spectroradiometer (MODIS) onboard the NASA Aqua platform was used, i.e. the 8-day composite product (MYD11A2, version 6 Wan et al. (2015)). For this work we only analysed the LST at around 13:30 local time during summer months (June, July, and August) from the years 2002-2011. The LST data set was then processed to get multi-annual summer mean LST following the method used in (Zhou et al., 2017).

Auxiliary data considered in this work include vegetation, background climate, topography, water bodies, as well as urban impervious density.

The vegetation information was extracted from MODIS EVI data (MOD13Q1, version 6, Didan (2015)). We downloaded the 250m 16-day composite product during all summer months from the years 2002-2011 and calculated the multi-annual average of the summer EVI.

Regarding the background climate conditions, the multi-annual average of summer precipitation, summer daily maximum 2m temperature, and summer 10m wind speed were calculated based on the corresponding monthly values from two data sets. The monthly precipitation and daily maximum air temperature during summertime from 2002-2011 were taken from CHELSA (climatologies at high resolution for the Earth's land surface areas) climate data set. CHELSA is based on a quasi-mechanistical statistical downscaling global reanalysis and global circulation model output (Karger et al., 2017) and has a resolution of 30 arc seconds (∼1km). It is hosted by the Swiss Federal Institute for Forest, Snow

and Landscape Research (WSL) and freely available at https://chelsa-climate.org/. The monthly 10m wind speed data set comes from the German Weather Service (Deutscher Wetterdienst, DWD) Climate Data Centre. This data set consists of gridded monthly mean near-surface (10m) wind speed values (Brinckmann, 2016) for Europe, and it was created by the project DecReg/MiKlip (Brinckmann et al., 2015) using an interpolation model which combines observation data and reanalysis data. The data set covers the period of 2001–2010 and has a resolution of 0.044° (∼5km). Similar to the precipitation data, only values from summer months were processed.

Another data source is the Copernicus Land Monitoring Service (CLMS, https://land.copernicus.eu/) funded by the European Union. From CLMS we downloaded the Imperviousness Density 2006 (IMD2006) at 20m resolution, and the European Digital Elevation Model (EU-DEM, version 1.0) with 25m resolution, as well as the CLC2006 at 100m resolution. We aggregated the IMD2006 and EU-DEM data to a coarser resolution of 250m by assigning each coarse cell the mean value from the fine cells it covers. The CLC2006 was first reclassified into binary water/land map according to whether the cells belong to the level-1 class "Water" (which includes water courses, water bodies, coastal lagoons, estuaries, sea and ocean, see (Büttner et al., 2012)). The binary map was then resampled to a 250m resolution with each coarse cell receiving a value of water surface fraction.

To overlay the various quantities, all the processed data sets were reprojected to the sinusoidal coordinate system as used by the LST data set.

2.2. Methods

2.2.1. SUHI calculation

We follow a similar methodology as Peng et al. (2012) and Zhou et al. (2013, 2017). First we apply the City Clustering Algorithm (CCA) (Rozenfeld et al., 2008, 2011; Fluschnik et al., 2016) to the UMZ2006 map, with the parameter $l = 250$m, to assign all cells which are no more than 250m apart from each other to the same urban cluster. Then we identify the 5,000 largest urban clusters (in terms of area) and the centroid location of each cluster (indicated in Fig. 1(h)). For each of the selected urban clusters, a boundary area with approximately the same size as the urban cluster is created following the method used in (Zhou et al., 2013). Cells that have a water surface fraction over 50% or belong to other urban clusters are excluded when creating the boundary area. Some example urban clusters and the corresponding boundary areas are shown in Fig. 1(a-f). Last we define the SUHI intensity (°C) as $\Delta T = \overline{T}_u - \overline{T}_b$, where $\overline{T}_u$ and $\overline{T}_b$ are the average LST of the urban cluster and of the boundary area, respectively.

2.2.2. Other variables extraction

Analogously, for each urban cluster we calculate the difference between the average value of water surface fraction, summertime EVI, and elevation of the urban area and the corresponding average value of the boundary area, and denote them as $U_{\Delta Wat}$, $U_{\Delta Veg}$, $U_{\Delta Ele}$ (m), respectively.

Moreover, we calculate the average value (summer time if applicable) of elevation, EVI, wind speed, precipitation, and maximum temperature within each boundary area and denote

them as background biophysical factors B_{Ele} (m), B_{Veg}, B_{Win} (ms^{-1}), B_{Pre} (mm) and B_{Tmx} (°C), respectively. As an important factor controlling the solar radiation, the latitude of the centre of mass for each urban cluster is also extracted and is denoted as B_{Lat} (°).

2.2.3. Geographically weighted regression model

In addition to ordinary least square (OLS) regression models, we performed a GWR to explore spatially varying relationships between the SUHI intensity and its explanatory variables. GWR is a non-parametric model that takes spatial non-stationary influences from associated factors into account by applying a locally weighted linear regression (WLR, see Jian et al. (1996)) for each observation with a subset of nearby observations (Fotheringham et al., 2003), and therefore allows parameters to vary across space. GWR usually takes the form

$$y_i = \theta_0(u_i, v_i) + \sum_k^n \theta_k(u_i, v_i) x_{k,i} + \epsilon_i \,, \tag{1}$$

where n is the number of independent variables; i denotes the ith observation; (u_i, v_i) is the coordinate of the ith location; $\theta_0(u_i, v_i)$ is the constant intercept depending on the coordinate (u_i, v_i); y_i, $x_{k,i}$, and ϵ_i are dependent variables, independent variable and the error term respectively; and the coefficients $\theta_k(u_i, v_i)$ are varying conditionals of the observation locations (Nakaya et al., 2014).

Proximity of geographical positions can, to some extent, represent the similarity of climate condition, but not always. For example, two cities located in proximity to each other but on opposite sides of a ridge may largely differ in background climate, especially in the patterns of precipitation and wind. One of our goals is to investigate the

climate control on the SUHI. Therefore, instead of a common GWR that takes only geographical location (u, v) as coordinates into account for Eq. (1), in this work we project the 5,000 cities into a 6-dimension space using their corresponding background biophysical factors, namely B_{Pre}, B_{Tmx}, B_{Veg}, B_{Win}, B_{Ele}, and B_{Lat} – forming a kind of *climate space*. A similar application of GWR can be found in (Hooker et al., 2018). To remove the influence of the magnitude of different climate variables, the z-score normalisation is applied to each of them. The coordinate of the ith city in the constructed space will be $\vec{P_i} = \{z(B_{Pre})_i, z(B_{Tmx})_i, z(B_{Lat})_i, z(B_{Veg})_i, z(B_{Ele})_i, z(B_{Win})_i\}$. This way, the distance between city i and j within the 6-dimension space can be calculated as $d_{i,j} = |\overrightarrow{P_i P_j}| = \sqrt{\sum_{k=1}^{6}(P_{i,k} - P_{j,k})^2}$.

For a city at location i, coefficients $\theta_{k,i}$ and ϵ_i are estimated by locally fitting a WLR that only takes its neighbouring cities within a certain distance L in the constructed climate space into account. In this work, the weight of city j is calculated using a tricube function, i.e. $w_j = (1 - (d_{i,j}/L)^3)^{1/3}$, with $d_{i,j} \leq L$. The local WLR leads to a set of coefficients $\{\theta_0(\vec{P_i}), \theta_1(\vec{P_i}), ..., \theta_n(\vec{P_i}), \epsilon_i\}$ and after application to each of the 5,000 cities we get 5,000 sets of coefficients. The GWR is implemented using the `R`-package "GWmodel" (Lu et al., 2014). An optimally fixed band width L is estimated using the leave-one-out cross-validation method, technical details can be found in Lu et al. (2014).

2.2.4. GUM index calculation

In the work of Li et al. (2020), a GUM index was found to be capable of capturing the influence of urban form on canopy urban heat island intensity. This index is calculated as

$\frac{1}{N}\sum_{j}^{N}\sum_{i\neq j}^{N} f(x_i)d_{ij}^{-\beta}$, where N is the number of cells of the considered urban cluster, d_{ij} is the distance between two urban cells i and j, and $f(x_i)$ is the function of the urban metric x influencing the temperature at site i. This was based on the hypothesis that an urban cell is affected by the warmth of other urban cells and this effect declines with the distance between them, also warmer urban cells have stronger effects on its neighbouring cells. Many studies show that the land surface temperature is highly related to characteristics like impervious surface fraction (Morabito et al., 2020; Li et al., 2011), building density (Song et al., 2020; Yin et al., 2018), vegetation fraction (Mathew et al., 2017; Li et al., 2011; Zhou et al., 2014), etc. Particularly, Li et al. (2018) revealed a linear relationship between land surface temperature and regionalised impervious surface area. Therefore, in this work we include impervious surface fraction and calculate our GUM index according to

$$D = \frac{1}{N}\sum_{j}^{N}\sum_{i\neq j}^{N} u_i^{\alpha} d_{ij}^{-\beta}, \tag{2}$$

where u_i is the impervious surface fraction of urban grid cell i, α and β are key exponent parameters. We calculate D for each of the 5,000 urban clusters and examine whether it also has an impact on the SUHI intensity.

3. Results

3.1. Influence of urban size and morphology on SUHI

We find that SUHI intensity ΔT is moderately related to urban area A, see supplementary Table S1 and Fig. S1. There is roughly a linear relationship between ΔT and logarithmic A, which is consistent with previous studies (Zhang et al., 2012; Zhou et al., 2017; Li et al.,

2017). This implies that with same amount of urban area increment, a larger city tends to experience a smaller increase in SUHI intensity. However, this does not mean it is preferable to have urban expansion concentrated in large cities, as the cost from heat stress is a super-linear function of temperature and population size (Estrada et al., 2017; Krummenauer et al., 2019).

Regarding the urban morphology, the relationship between GUM index D and SUHI intenisty ΔT varies with the exponents α and β. Specifically, when $\alpha = 0.2$ and $\beta = 2$, D has a high correlation with ΔT, the Pearson correlation coefficient r reaches 0.64 (see supplementary Table S1 and Fig. S1 for the correlation and the spreading range of D). In Fig. 1(a-f) we show six example urban clusters with approximately the same area and corresponding D values when $\alpha = 0.2$ and $\beta = 2$ are used. It can be seen – when keeping the urban size constant – compact cities generally tend to have a larger D value. However, it has to be noted that this does not always hold as the impervious surface density also has an influence on D. As D is a very complex indicator which involves the spatial configuration of the urban cells as well as their built-up density, without some preconditions (i.e., same size or same impervious surface fraction), it is hard to get the conceptual impression whether one city is more compact than another through comparison of their value D. Generally, cities with rounder shape and higher impervious density will have larger D value. Fig. 1(g) shows ΔT against D (with $\alpha = 0.2$, $\beta = 2$) of some example cities with approximately the same area ($15 \pm 0.06\text{km}^2$, for other areas sizes, see supplementary Fig. S2). As shown, ΔT is positively related to the D value despite the fluctuation that might be attributed to the influence from other factors, in particular background climate and water bodies.

This implies that more compact and denser urban structures tend to have higher SUHI intensities. Moreover, urban heat mitigation strategy through optimising urban morphology should carefully consider the local scale context sensitivity of SUHI, as this neighbourhood effect can impact the city scale thermal environment when aggregated.

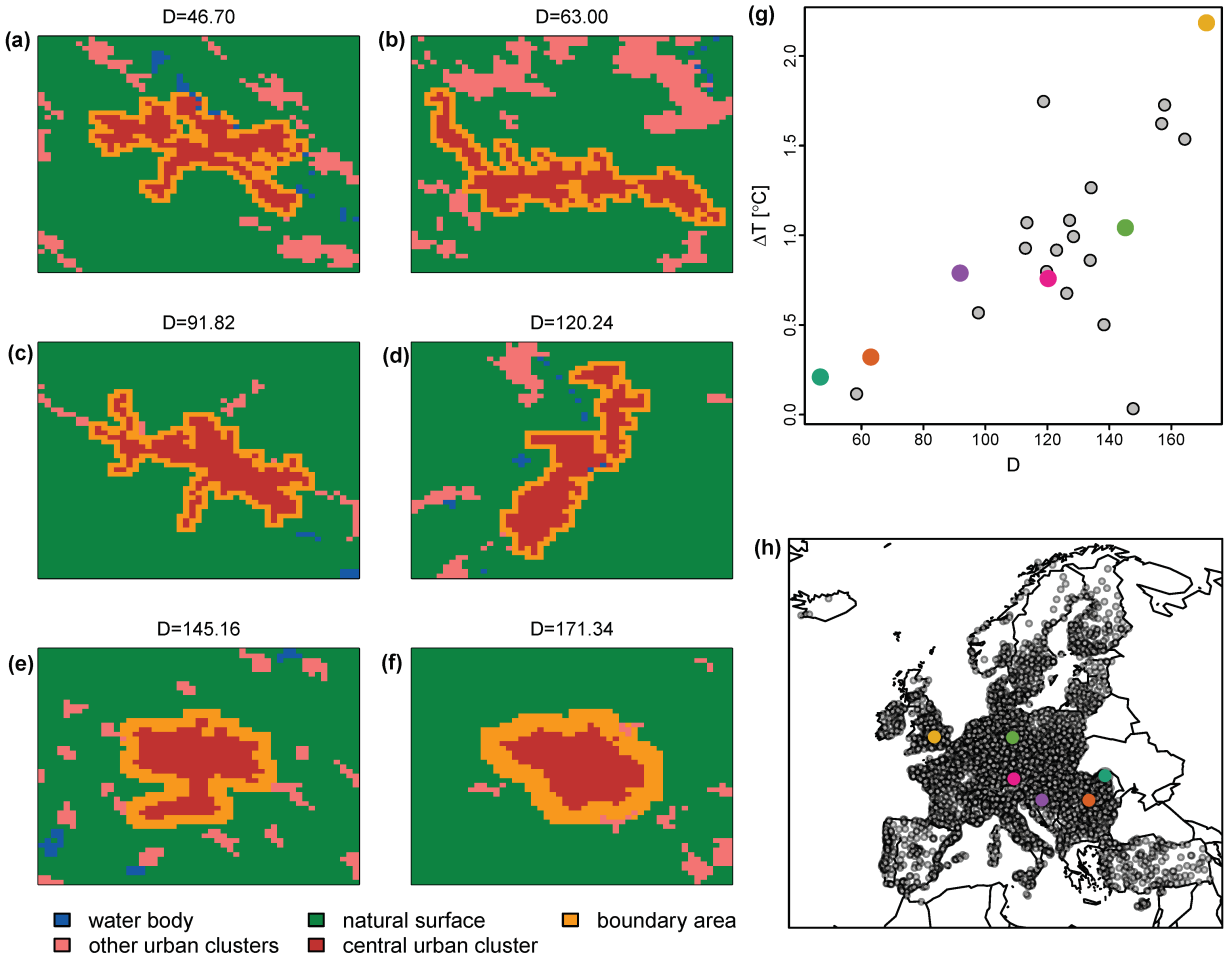

Figure 1: **Some example urban clusters with approximately the same size, their boundary areas, as well as the corresponding D values and SUHI intensities.** Panel (**a-f**) show the clusters of the highlighted clusters in panel **g**, the size of this six clusters range from 14.94-15.06 km^2. Panel (**g**) shows the SUHI intensity against D value of 41 urban clusters with approximately the same size, where the points in colours represent the clusters in Panel (**a-f**). Panel (**h**) shows the spatial locations of all 5,000 clusters with the clusters in panel (**a-f**) highlighted in colours.

Similar to the approach used by Li et al. (2020), we regress ΔT with A and D as:

$$\Delta T = a_1 \ln A + a_2 D + a_3 \quad \text{with} \quad D = \frac{1}{N} \sum_{j}^{N} \sum_{i \neq j}^{N} u_i^{\alpha} d_{ij}^{-\beta}, \tag{3}$$

where a_1, a_2, a_3 are parameters. Fitting Eq. (3) using the data of all 5,000 cities with different combinations of α and β, we obtain varying R^2 (see Fig. 2).

We find $\alpha = 0.2$, $\beta = 2$ leads to best results in terms of R^2 (which is 0.40). These values differ from the ones found by Li et al. (2020) for canopy UHI intensity ($\alpha = 0.5$, $\beta = 1.5$). As canopy and surface UHI involve different processes, we cannot directly compare them, but it is still worth thinking about possible implications for the conceptualisation. A larger β value implies that the neighbourhood influence of the LST decays faster and thus has a shorter range than the canopy layer temperature. It is plausible that air temperature has a smoother spatial gradient than the LST as the former is more easily influenced by energy and air flow. This indicates that at local scale SUHI is less context sensitive than CUHI. For SUHI, the influence from nearby urban cells decays very fast with increasing distance. Thus, the neighbourhood influence can only reach a rather small range.

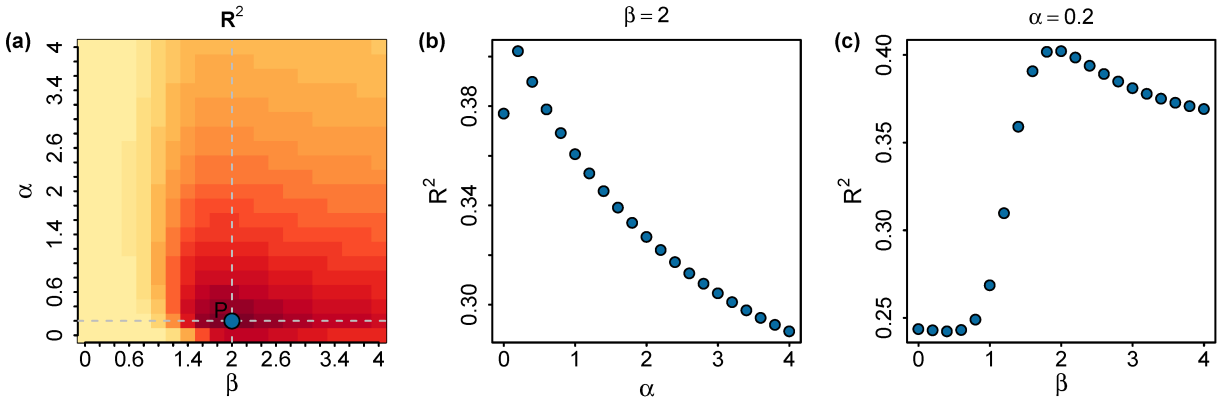

Figure 2: **The R^2 of the OLS fitting on Eq. (3) as a function of α and β values.** (**a**) 2D visualisation, deeper red for higher R^2. (**b**) R^2 profile when $\beta = 2$. (**c**) R^2 profile when $\alpha = 0.2$.

The coefficients from the fitting for Eq. (3) with $\alpha = 0.2$, $\beta = 2$ are also shown in Table 1,

all of them are above 95% significance level. It is also worth mentioning that although D and $\ln A$ are not independent, a variance inflation factor of 2.21 suggests an insignificant impact of the co-linearity between $\ln A$ and D on the reliability of the regression, as usually a value > 10 is considered severe (Neter et al., 1996).

To avoid ambiguity, the GUM index D was calculated with $\alpha = 0.2$, $\beta = 2$ for the remainder of this paper.

3.2. Influence of additional urban factors

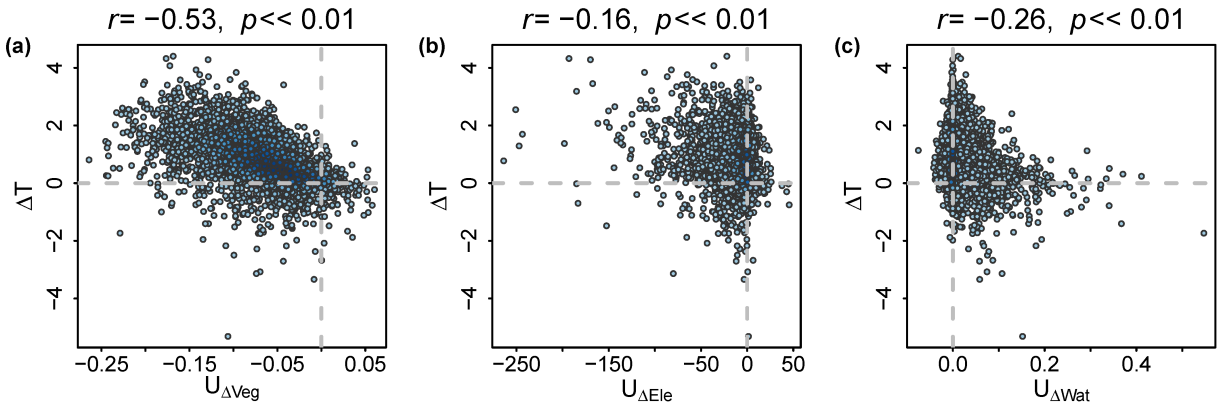

Figure 3: ΔT **against additional urban factors.** (a) $U_{\Delta Veg}$, urban-boundary difference in EVI, (b) $U_{\Delta Ele}$, urban-boundary difference in elevation, and (c) $U_{\Delta Wat}$, urban-boundary difference in water surface fraction. On the top of each panel Pearson Correlation (r) and p value are listed.

Although we obtain a slightly higher R^2 when using Eq. (3) as regression with less parameters compared to the multivariate linear regression in (Zhou et al., 2017), there is still a large part of variance of ΔT that is not explained by $\ln A$ and D (see supplementary Fig. S5 and Fig. S3). This is due to the influences from many other factors. As reported in various studies, water bodies (Zhou et al., 2014; Yin et al., 2018; Wang et al., 2019), vegetation

(Zhou et al., 2011, 2014; Yu et al., 2018), and altitude (Mathew et al., 2017; Guo et al., 2020) are also associated with SUHI intensity. This is further confirmed by our results, as we can see in Fig. 3, there is a statistically significant correlation between ΔT and urban-boundary difference in EVI ($U_{\Delta Veg}$), in water surface fraction ($U_{\Delta Wat}$), and in elevation ($U_{\Delta Ele}$). In general, cities with less vegetation, lower altitude, and less water surface than their surroundings, tend to experience stronger SUHI intensities. This is consistent with previous studies on the contributions of green and blue infrastructure to urban heat mitigation. Our results particularly underpins the effect of urban greening on SUHI reduction. Including these factors in Eq. (3) and using the regression

$$\Delta T = b_1 \ln A + b_2 D + b_3 U_{\Delta Wat} + b_4 U_{\Delta Veg} + b_5 U_{\Delta Ele} + b_6 \,, \tag{4}$$

we obtain coefficients detailed in Table 1, where all coefficients are above 99% significance level. Including $U_{\Delta Wat}$, $U_{\Delta Veg}$, and $U_{\Delta Ele}$ in the regression model, Eq. (4) achieved a clear improvement of R^2 and of root mean square error (RMSE) in contrast to Eq. (3).

3.3. Sensitivity of SUHI to regional climate context

Besides the intrinsic urban factors that denote the urban-boundary differences due to land surface modification from urbanisation, SUHI has been reported to be associated also with various background biophysical factors such as precipitation, temperature, humidity, wind speed, latitude, and altitude, among which precipitation (Peng et al., 2012; Zhao et al., 2014; Manoli et al., 2019), and temperature (Peng et al., 2012; Zhou et al., 2016; Manoli et al., 2019) seem to be most documented. Therefore, SUHI is also context sensitive to regional climate background.

This regional scale context sensitivity can be seen in Fig. 4. When plotting ΔT against each of the 6 background factors, ΔT has a clear correlation with B_{Pre} and with B_{Tmax}, which is consistent with previous studies (Peng et al., 2012; Zhou et al., 2014). The positive relationship between ΔT and B_{veg} can be explained by the tendency of boundary areas with higher EVI to be generally cooler due to stronger evapotranspiration. There is a positive correlation between ΔT and B_{Lat}, which is consistent with the finding in (Li et al., 2017). However, beyond a certain latitude, ΔT seems to decrease when latitude increases. Our results do not show statistically significant correlation between ΔT and B_{Ele} or B_{Win}, which might be due to the correlation being too weak to stand out from noises caused by other factors. The correlation between the residuals from the regression of Eq. (4) and the six background biophysical factors (as shown in supplementary Fig. S4) indicates that the explanatory power of the regression model could be improved by including these background factors. In principal, one could just extend the regression by including them in the multivariate linear model. However, those background factors are likely to interact with urban factors and the interactions are not necessarily linear (Li et al., 2019; Manoli et al., 2019). Moreover, It is plausible that the dependence of SUHI on climate context results from the role of background climate in controlling how SUHI respond to urban factors.

3.4. Geographically Weighted Regression

We are interested in exploring how the influence of urban factors on the SUHI intensity varies regionally across the climate context. To this end, we apply the GWR

$$\Delta T_i = \theta_0(\vec{P}_i) + \sum_k^5 \theta_k(\vec{P}_i) x_{k,i} + \epsilon_i \,, \tag{5}$$

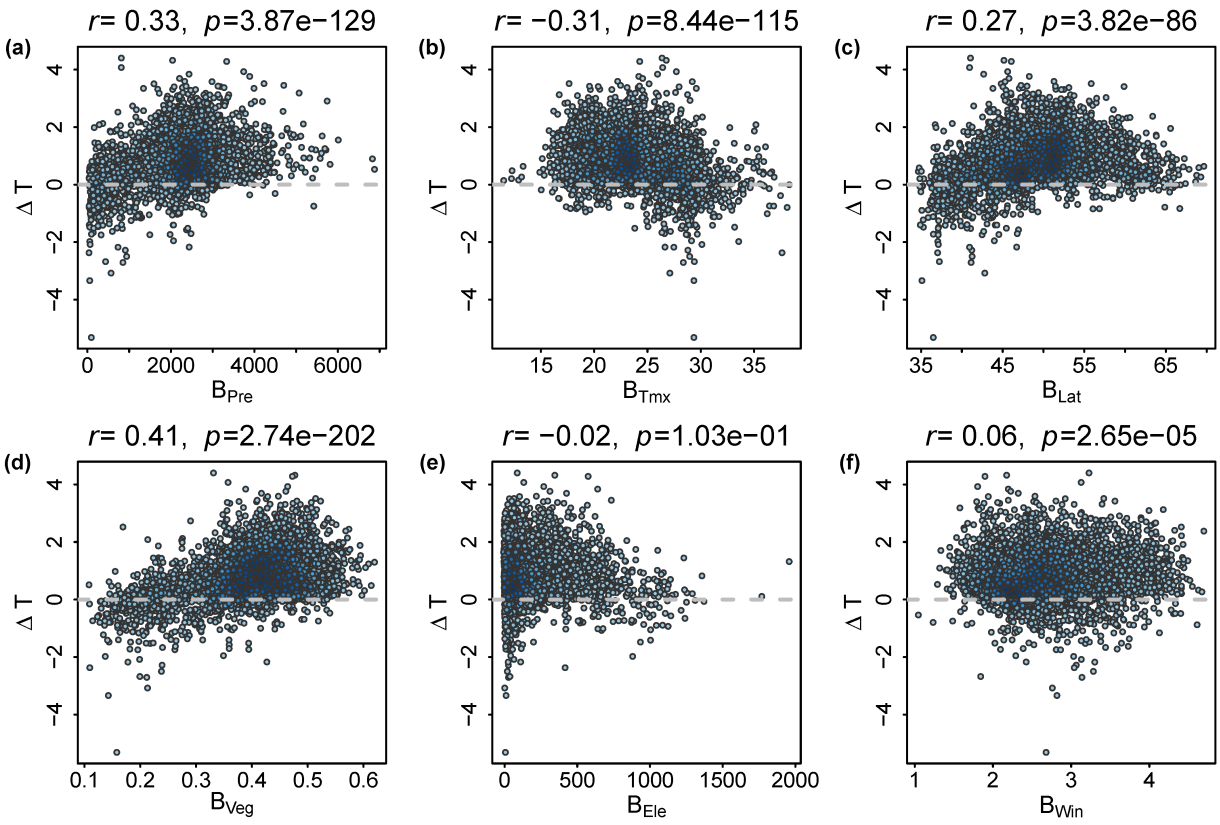

Figure 4: **SUHI intensity ΔT against background biophysical factors:** (a) summer precipitation B_{Pre}. (b) summer mean maximum temperature B_{Tmx}. (c) latitude B_{Lat}. (d) summer EVI of boundary area B_{veg}. (e) elevation B_{Ele}. (f) summer 10m wind speed B_{Win}. r and p on the top of each panel indicate the Pearson correlation coefficient and the significant level of the plotted variables.

where $\theta_0(\vec{P}_i)$ is the intercept of the regression for the ith city, $x_{k,i}$ is the kth independent variable as that used in Eq. (4) of the ith city.

Fitting Eq. (5) leads to a set of coefficients $\{\theta_{0,i}, \theta_{1,i}, ..., \theta_{5,i}, \epsilon_i\}$ for each of the 5,000 cities and thus we get 5,000 sets of coefficients. We notice that Li et al. (2017) applied GWR on 5,000 urban clusters across continental US based on their geographical location and then investigated the spatial variation of the relationship between SUHI and urban area. In our

work, the GWR is applied based on a constructed 6-dimension biophysical space in order to study the variation of the relationship between SUHI and various urban factors against each background biophysical factor.

The statistics of GWR results can be found in Table 1. Compared to the regression of Eq. (3) and Eq. (4), it shows apparent improvement in R^2 and RMSE. This indicates that the relationship between SUHI and urban factors is not stationary across the climate context. The density plot of residuals from all the three regression models are also compared in supplementary Fig. S5.

Table 1: **Comparison of OLS fitting and GWR fitting.** Numbers within the bracket are the standard deviations of corresponding values. AICc is calculated following Zhou et al. (2016).

model	Eq. (3)	Eq. (4)	GWR
coef. $\ln A$	5.13×10^{-2}	0.17	$5.44 \times 10^{-2}(0.10)$
coef. D	1.31×10^{-2}	6.15×10^{-3}	$1.09 \times 10^{-2}(6.05 \times 10^{-3})$
coef. $U_{\Delta Wat}$	–	-6.00	-4.90 (2.03)
coef. $U_{\Delta Veg}$	–	-6.53	-4.27 (3.24)
coef. $U_{\Delta Ele}$	–	-3.90×10^{-3}	$-5.69 \times 10^{-3}(2.21 \times 10^{-3})$
intercept	-0.90	-0.79	-0.86 (0.21)
R^2	0.40	0.55	0.74
RMSE	0.63	0.54	0.41
AICc	1161.56	395.67	-979.27

We also plot the residuals of the GWR model against the background biophysical factors

as in Fig. 5. Compared to the supplementary Fig. S4 where residuals from the linear regression of Eq. (4) are plotted against the background biophysical factors, we can clearly see that the residuals from the GWR model are much less correlated with background factors. This implies that the variation of coefficients of the GWR model to a large extent resolves the sensitivity of SUHI to regional climate context and the background factors impact SUHI through affecting the way that SUHI responds to urban factors. This varying relationships also suggest that the cost-efficiency of different urban heat mitigation strategies is highly dependent on climate context. Special caution should be exercised when extending lessons learned from one city to another, especially when they share less in common in background climate.

3.5. Non-stationary influences of urban factors governed by background climates

The GWR model gives flexibility to the coefficients of the regression. Thus it takes the non-stationary associations of different factors with SUHI into consideration. As this non-stationarity is also believed to be modulated by climate context, we apply the GWR based on a constructed climate space. In this way, the local regression is applied on the clusters of cities with most similar background climate, so that the influence from background factors is minimised and the statistical contribution of each urban factor can be examined regionally.

In the supplementary Table S2 we show the Pearson correlation coefficients between the GWR coefficients and the background biophysical factors. Some background factors, such as precipitation B_{Pre}, air temperature B_{Tmx}, latitude B_{Lat}, and vegetation condition B_{Veg}, have a clear correlation with GWR coefficients, where the highest correlation coefficient reaches

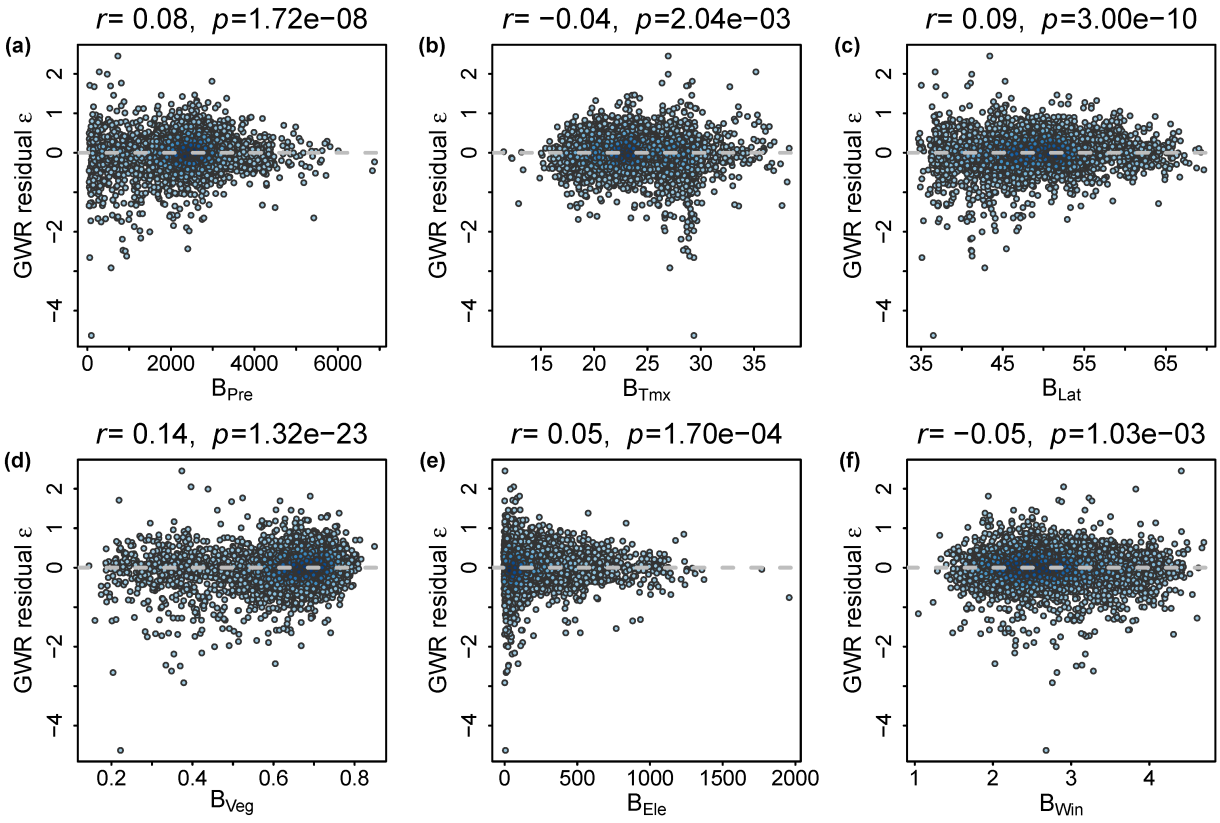

Figure 5: **residuals from GWR model against background factors:** (a) summer precipitation B_{Pre}. (b) summer mean maximum temperature B_{Tmx}. (c) latitude B_{Lat}. (d) summer EVI of boundary area B_{veg}. (e) elevation B_{Ele}. (f) summer 10m wind speed B_{Win}.

0.84, indicating the strong influence of the background factors on the variation of the GWR coefficients. This is not surprising as in previous studies it has been found that precipitation and temperature show a strong control on daytime SUHI (Zhao et al., 2014; Zhou et al., 2016; Manoli et al., 2019). We can also see that some coefficients show a strong correlation with more than one background factor. However, without comprehensively studying the underlying dynamics it is difficult to prioritise one background factor over another.

We plot each GWR coefficient against its highest correlated background factor in Fig. 6.

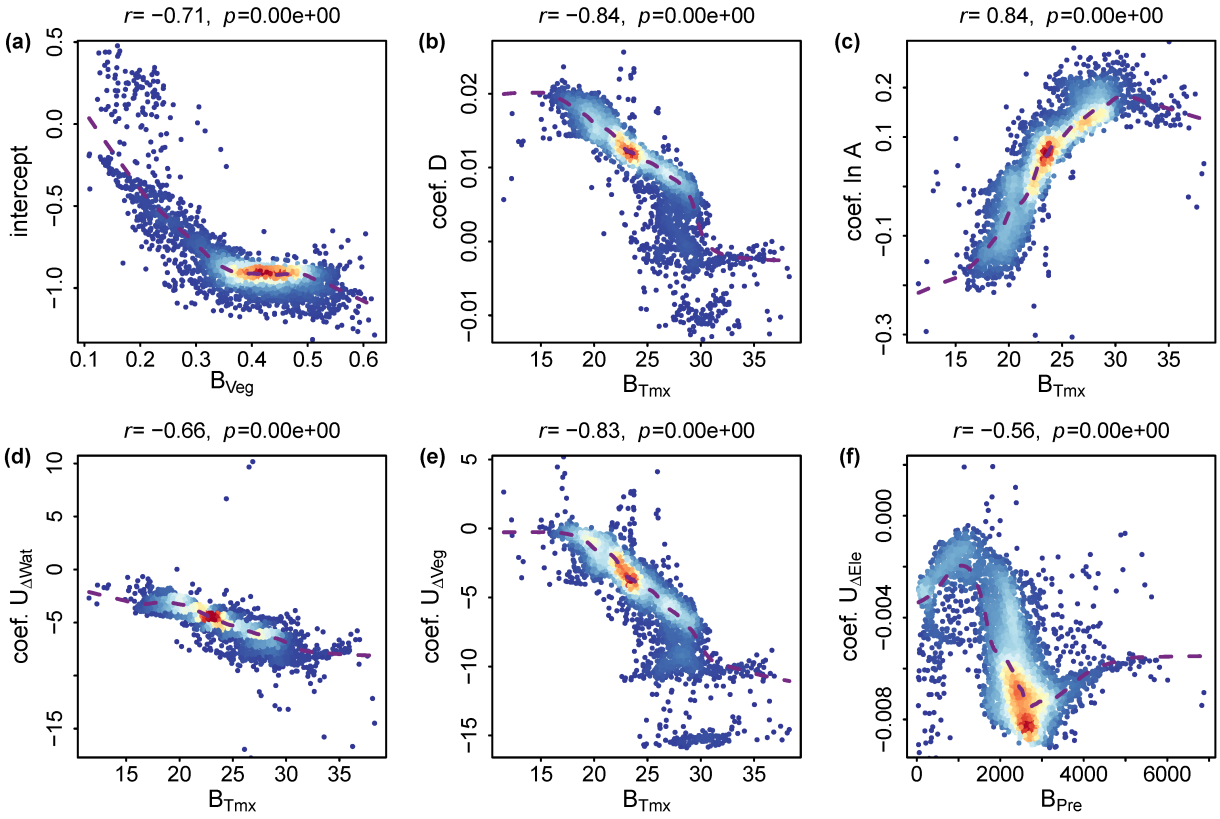

Figure 6: **Relationship between some coefficients from GWR and background climate factors.** The dashed lines are a guide to the eye from LOWESS (Locally Weighted Scatterplot Smoothing) regression.

Despite some noise, all the GWR coefficients except that of ln A generally maintain the sign while varying in quantity. This implies that strategies for SUHI reduction through changing one of the urban factors might show different efficiency under different biophysical context – the consequence seems to be consistent qualitatively. Our results indicate that when other urban factors remain constant, urban sprawl tends to cause smaller SUHI increment for cities in northern European, or more specifically, in colder, wetter, windier and more vegetated areas (see supplementary Fig. S6). Likewise, with similar preconditions we can infer that a colder, wetter, windier and more vegetated context would favour the contribution of urban

morphology D to SUHI, but weaken the contribution of water surface share difference $U_{\Delta Wat}$ and EVI difference $U_{\Delta Veg}$ (see supplementary Fig. S7-S9). However, a general trend on the variation of coefficient of elevation difference $U_{\Delta Ele}$ is more complex and can hardly be drawn qualitatively (supplementary Fig. S10).

3.6. Nonlinear model considering climate context sensitivity of SUHI

In principle, all the factors used in this study can be fed into a multiple linear regression model of the form

$$\begin{aligned}\Delta T =& c_1 \ln A + c_2 D + c_3 U_{\Delta Wat} + c_4 U_{\Delta Veg} + c_5 U_{\Delta Ele} + \\ & c_6 B_{Pre} + c_7 B_{Tmx} + c_8 B_{Veg} + c_9 B_{Ele} + c_{10} B_{Lat} + c_{11}\,,\end{aligned} \tag{6}$$

and with more variables we could obtain a RMSE of 0.46, which is better than that of fitting Eq. (4), but still larger than the RMSE from the GWR model. As there are complex dynamic processes controlling the SUHI, the factors, both from urban metrics and from background biophysical factors, tend to interact with each other non-linearly. A linear regression model certainly cannot capture the interacting effect as it is just a combination of the linear approximation for each factor.

However, although regression with the GWR model has a higher accuracy, it does not necessarily mean the GWR model has better practical usability. The parameter estimation of GWR comes from local fitting with location specific information, which limits the generality of the model and a better understanding cannot be obtained without further exploration. Instead, by examining the linkages between the variation of the GWR coefficients of each urban factor and background factors, the effect of interactions between the background

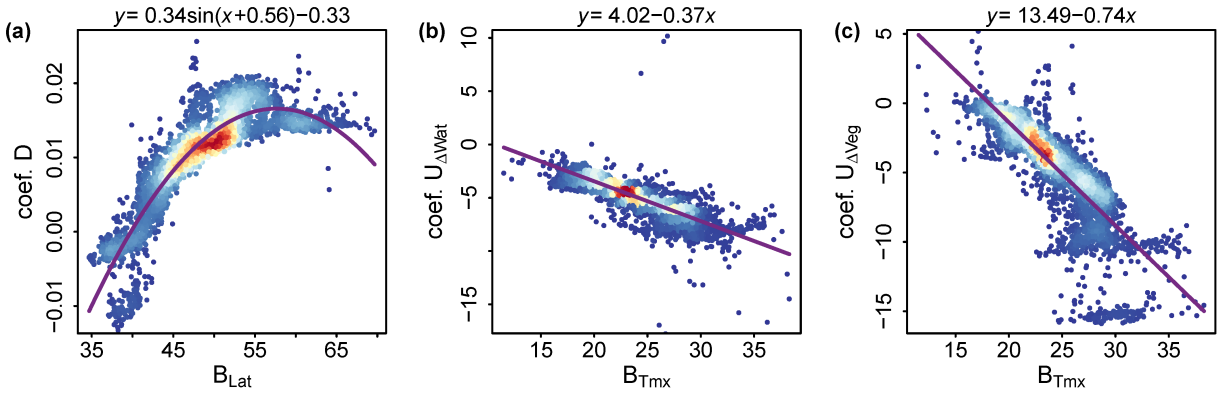

Figure 7: **GWR coefficients as a function of background biophysical factors.** The solid line is the fitted curve as expressed on top of each panel.

factors and urban factors can be quantitatively studied. This could help to formulate a more general regression model to estimate the SUHI intensity. For example, in Fig. 7(a), after having a careful look at the relationship between the GWR coefficients of D and the latitude B_{Lat}, and considering that the total solar irradiance should be a trigonometric function of the latitude, we could fit the coefficient of D with latitude B_{Lat} in the form of $e_1 \sin(x + e_2) + e_3$. Similarly, for the coefficient of $U_{\Delta Wat}$ and the coefficient of $U_{\Delta Veg}$, we find they can be roughly expressed as a linear function of B_{Tmx}. With this knowledge, we extend the global linear regression of Eq. (4) by replacing the coefficients of D, $U_{\Delta Wat}$ and $U_{\Delta Veg}$ with functions of the above mentioned climate factors

$$\begin{aligned}\Delta T =& d_1 \ln A + [d_2 \sin(B_{Lat} + d_3) + d_4] D + \\ & d_5 B_{Tmx} U_{\Delta Wat} + (d_6 B_{Tmx} + d_7) U_{\Delta Veg} + d_8 U_{\Delta Ele} + d_9,\end{aligned} \tag{7}$$

and we obtain a RMSE of 0.44 from fitting Eq. (7), which is better than the fitting with all considered factors and very close to the RMSE from the GWR model.

In supplementary Fig. S5, we compare all the regression models mentioned in this work in

terms of their residuals, RMSE, and AICc. It can be seen that the GWR model outperforms all other models, which is followed by the nonlinear regression of Eq. (7). Particularly, if we compare regression of Eq. (7) with that of Eq. (6), a smaller RMSE is achieved with fewer parameters when some interactions between the factors are taken into account. This shows that the GWR model can help to find a better SUHI prediction model as it enables us to explore the interactions between some factors. Thus, the model based on Eq. (7) is preferable as a tool for SUHI prediction and may have even more implications for SUHI assessment under the scenarios of future urbanisation and climate change, as the model uses both urban factors and background biophysical factors as predictors for SUHI intensity.

It has to be noted that the nonlinear model in the form of Eq. (7) may not be the optimal one as different background factors can be introduced with functions taking different forms (see Supplementary Fig. S6-S10). Rather, we illustrate here how the GWR model can help to obtain a better model that captures the context sensitivity of SUHI to regional climate.

4. Discussion

4.1. Urban morphology and SUHI

Taking the similar form as the one proposed in (Li et al., 2020) which was used to link canopy UHI intensity to urban morphology, the GUM index in this work turns out to be also an effective indicator to capture the relationship between SUHI intensity and urban morphology. Our results agree with previous studies on the contribution both of 2D urban compactness (Zhang et al., 2012; Zhou et al., 2017) and of the urban density (Zhang et al., 2012; Li et al., 2018; Song et al., 2020) to SUHI intensity. Compared to

various metrics for quantifying 2D urban morphology in previous studies, our approach underlines the importance of looking at cities from a 3D perspective, as 2D urban morphology neglects the influences from urban development within already urbanised areas (i.e., urban densification). The GUM index combines the 2D geometry of the urban clusters and the spatial heterogeneity of the impervious density inside, where the latter is key to capture the local scale context sensitivity of SUHI and could affect the city scale SUHI when aggregated. It can serve as an effective predictor for SUHI intensity assessment in view of urbanisation which usually involves both densification and sprawl.

Also similar as in (Li et al., 2020), generally the GUM index indicates that cities with higher compactness and density tend to have stronger SUHI. However, specific implications regarding the influence of urban morphology on SUHI intensity could only be interpreted with some preconditions. For example, assuming the urban area A remains unchanged and the impervious surface fraction u is homogeneous within the urban cluster, the GUM index D degrades to a indicator that measures the compactness of the 2D urban morphology. Under this circumstance, it implies that from a 2D perspective cities with rounder shape will have larger SUHI intensity.

In principal, the weight function used in calculating the GUM index D should not be limited to a function of only urban impervious surface fraction u. Other indices like urban canyon geometry, building density, water surface fraction, vegetation fraction can also modulate the LST at local scale (Zhang et al., 2012; Mathew et al., 2017; Song et al., 2020; Liu et al., 2021a). Therefore, a more complex indicator that considers the heterogeneous configuration of and the interaction between these indices within the urban cluster probably can

carry more prediction power on the resulted SUHI intensity. However, this requires much more effort and a more comprehensive understanding of the underlying biophysical processes (Manoli et al., 2019) through which the considered factors influence the LST. Future work in this direction is needed.

4.2. Drivers of SUHI

While it is easy to infer the statistical linkages between SUHI and related factors, revealing the causality is a very different challenge, especially given the fact that many natural and socioeconomic factors found to be associated with SUHI are correlated among themselves. Therefore, efforts to identify the driving factors as well as their corresponding contribution to SUHI might lead to discrepant and sometimes contradicting conclusions. This is either due to the combination of factors chosen or due to the studied samples that are not suitable for factor separating.

For example, although the association between SUHI and urban area has been examined by studies at different scales (Peng et al., 2012; Zhou et al., 2017; Li et al., 2017), community consensus over the understanding of this statistical correlation still lacks. Peng et al. (2012) find no obvious effect of urban size on the SUHI for 419 global big cities but significant positive correlation exists for 56 European cities, they surmise that the effect of urban size at the global scale might be masked by the differences in background climate or economic development. Zhou et al. (2017) take a logarithmic function to capture the relationship between SUHI and urban size, meanwhile they also illustrate the suitability of a log-logistic function as an alternative. Li et al. (2017) point out that although the log-linear relationship

between SUHI and urban area exists across the continental US with local variation attributed to contextual biome, urban area is only a useful surrogate of other factors determining SUHI instead of being a major direct driving factor. This is plausible especially considering the fact that urban area is strongly correlated with population size, infrastructure size, energy consumption, and many other city-level socioeconomic metrics via well documented urban scaling laws (Gudipudi et al., 2019).

For other factors, attempts to quantify their contribution as a driving factor of UHI face similar problems as when studying urban area as driving factor. Thus, without a general understanding, results from one region carry little application capability for another region, or at least, it is risky to extrapolate the implication from one study beyond space and time. Therefore, causal attribution requires more than statistical analyses between SUHI and the potential driving factors. A combination of a statistical with a proper analytical attribution model (Li et al., 2019; Chen et al., 2020) based on energy balance could help to advance our understanding of the SUHI and thus guide the inference of causality between SUHI and related factors. For instance, in the work by Manoli et al. (2019), various urban characteristics and aerodynamic properties are expressed using urban population size with resort to the urban scaling law and a coarse-grained model has been developed to foster the general understanding of SUHI and the model has been shown capable of explaining the seasonal SUHI hysteresis (Zhou et al., 2013; Manoli et al., 2020).

Partitioning the contribution from different factors to the SUHI is beyond the scope of this work. With the observed results, we could only draw the implication that in general, larger, more compact cities with less water surface, less vegetation and lower than

surrounding area altitude tend to experience a stronger SUHI. When taking these factors as predictors, the regression model works quite well. With the help of the GWR model, we are also able to see how the influence from each urban factor vary across background biophysical space. Generally, cities in Europe with colder, wetter, windier and more vegetated background tend to experience stronger SUHI increment due to increased compactness, but less SUHI reduction due to increased water surface and vegetation. Moreover, with the help of GWR model, we are able to build a more general nonlinear model that can take the context sensitivity of SUHI at both local and regional scale. This model could serve as useful quantitative tool for SUHI intensity assessment with different urbanisation scenarios and climate change scenarios as input.

4.3. Possible explanation of outliers

In addition to the factors considered in this study, many others like building density, albedo, humidity, wind direction, water proximity also play a role in the formation of SUHI (Peng et al., 2012; Oke et al., 2017), and we assume they can be neglected. Although the urban-boundary differences in water surface fraction and in elevation are considered in the regression model, they cannot fully capture the influence of water proximity and topography on SUHI.

In the supplementary text, by further analysing the cities with large errors ($|\epsilon| > 1$) of the GWR regression, we examine qualitatively how water proximity affect SUHI intensity of a city in some cases. Specifically, the proximity to nearby large water body and particularly, whether urban area is closer to water body than boundary area, can strongly influence their

difference in the received cooling effect (see Fig. S13). However, a proper indicator is in need to quantitatively capture this difference. Based on fine Landsat LST image, Wang et al. (2019) proposed a gravitational water index that measures the cooling effect from nearby water cells received by grid cell i as $GWI_i = \sum_{d_{ij}<R} \frac{A_j}{d_{ij}^{\gamma}}$, where A_j is the water area in cell j. This index considers the influence from other water surface within a certain distance R for each grid cell and the influence decays as a power-law function of the distance to the water surface. The gravitational water index was found to be able to explain the LST variation at different grid scales. Probably a similar index can be developed for quantifying city-scale influence from nearby water surfaces and it may be an effective predictor of SUHI intensity. However, as two major parameters of the gravitational water index, the exponent γ which defines how stark the cooling effect decays and the distance threshold R up to which the cooling effect can reach, are very likely to vary even within one city (Du et al., 2016), not to mention for whole Europe. Therefore, it is beyond our scope to verify such an index or its variant.

Moreover, we also observe some cities with a larger positive prediction error which are situated in a valley like in Fig. S12(b-c). This might imply that topography also plays a role by influencing the heat dissipation. Although the GWR model already showed that cities with larger elevation differences between urban and boundary area tend to have stronger SUHI, the topography characteristics as in Fig. S12(b-c) may not be simply quantified by elevation differences. Future effort for proper indicators that consider the spatial pattern of the topography can help with a better SUHI intensity estimation model.

5. Conclusion

In this study we investigate the summer daytime SUHI intensity of the 5,000 largest urban clusters in Europe and demonstrate the capability of the proposed GUM index as an effective predictor of SUHI intensity. The GUM index is designed to capture the context sensitivity of SUHI to local neighbourhood effect and it quantifies the urban structure from a 3D perspective. The regression model can be improved when taking other urban factors like urban-boundary difference in vegetation, in water surface fraction and in elevation into account. The regression models show that generally larger, denser, and more compact cities tend to experience stronger SUHI, whereas cities with larger urban-boundary difference in elevation, vegetation cover and water surface cover tend to have lower SUHI intensity.

To explore the sensitivity of SUHI to regional climate context, we then project all the cities in a 6-dimension climate space constructed using six background biophysical factors. The GWR model is applied based on the constructed climate space to explore how the coefficients vary against different background biophysical factors. The GWR model shows further considerable improvement in terms of R^2 and RMSE compared to multivariate linear models. By enabling the variation of coefficients, the control from the background climate on the non-stationary contribution of different urban factors to SUHI can be captured by the GWR model. As influence of different urban factors on SUHI is context sensitive to regional climate, extrapolating knowledge from one area to another should be done with great caution, especially between areas with disparate climates.

Investigating how the GWR coefficients vary against different background biophysical

factors, we demonstrate how to replace the coefficients a in multivariate linear model with the background factors and propose a nonlinear model that can capture some of the interaction between the urban factors and the background biophysical factors. It carries fewer parameters but outperforms multivariate linear models. The nonlinear model considers the context sensitivity of SUHI at both local and regional scale, it is a more general model that can be used for SUHI assessment under different urbanisation and climate change scenarios.

Our results could provide useful information regarding urban heat reduction strategies, especially considering the ongoing rapid global urbanisation and climate change. A better urban development plan that takes the influence of urban morphology into account could benefit the urban thermal environment. Moreover, measures for urban heat mitigation should also consider the predicted climate change. As the climate context of a city may change in the future, heat mitigation strategies that are effective for a short term might show little efficiency for a long term.

Credit authorship contribution statement

Y. L. = conceptualisation, methodology, analysis, visualisation, and writing (original draft). B. Z. = conceptualisation, methodology, and writing (review and editing). M. G. = conceptualisation, methodology, and writing (review and editing). D. R. = Funding acquisition, conceptualisation, methodology, project administration, supervision, analysis, and writing (original draft, review and editing). J. P. K. = conceptualisation, methodology, supervision, writing (review and editing)

Declaration of competing interest

The authors declare that they have no known competing financial interests or personal relationships that could have appeared to influence the work reported in this paper.

Acknowledgements

We appreciate useful comments from L. Costa. Y.L. thanks China Scholarship Council (CSC) and Potsdam Graduate School (PoGS) for financial support. D.R. thanks the Alexander von Humboldt Foundation for financial support under the Feodor Lynen Fellowship. M.G. and D.R. are grateful to the Leibniz Association (project IMPETUS) for financial support.

Appendix A. Supplementary information

Appendix A.1. Influence of water body proximity on SUHI

To examine influence of water proximity on SUHI, we plot the spatial distribution of the residuals from the GWR model as in Fig. S12. Most of the cities with large errors ($|\epsilon| > 1$) of the GWR regression are located at the coast of the sea or a big lake. This might be due to the urban-boundary difference in received cooling effect of the breeze from large water bodies. This difference could be influenced by wind direction and the proximity to water bodies. The influence from wind speed and urban-boundary difference in water surface share can be captured by the GWR model, so we assume the cooling effect from nearby water bodies not considered in the regression model can explain large predicting errors, as the cooling effect of water bodies has been found to decay along the distance (Su et al., 2012; Du et al., 2016; Wang et al., 2019).

As an attempt to quantify the difference in water body proximity between urban area and boundary area, for each city we calculate the ratio of neighbouring water cells for both urban area and boundary area (namely the number of water cells adjacent to urban cells divided by the number of urban cells, and the number of water cells adjacent to boundary area cells divided by the number of boundary area cells, respectively) and take the difference in the ratios as an indicator. From the supplementary Fig. S13 we can see that the majority of the cities with large negative prediction errors ($\Delta T - \Delta T_{predicted} < -1°\mathrm{C}$) have a larger ratio of neighbouring water cells for the boundary area than for the urban area and a majority of the cities with large positive prediction errors ($\Delta T - \Delta T_{predicted} > 1°\mathrm{C}$) have a larger ratio

of neighbouring water cells of the urban area than of the boundary area. However, Fig. S13 also shows that a large difference in ratio of neighbouring water cells does not necessarily lead to a large prediction error. This means that a better indicator is needed to quantify the influence of water proximity on SUHI.

We explore the influence of water bodies rather qualitatively. In Fig. S12(d-i) we show the maps of some example urban clusters as well as their boundary areas. In the panels (d) and (e) the GWR prediction error is larger than 1 °C, which means the SUHI intensity is larger than the GWR model predicted. It might be due to their boundary areas which are relatively close to water compared to the urban clusters. For example, in panels (f)-(i) the predicted SUHI intensity is much larger than observed, as the GWR prediction error is always smaller than -1 degree. A possible reason is that urban clusters are much closer to water bodies than the corresponding boundary area, thus the urban clusters are exposed to more cooling. We find that similar to the examples in Fig. S12(f)-(i), most of the cities spreading in a strip shape along the coast of the sea or a lake, tend to have a larger negative prediction error. Whereas only a few exceptions exist, which might be because the influence from topography or the summer prevailing wind direction that does not favour the penetration of cool breeze into urban area.

Appendix A.2. Supplementary figures and tables

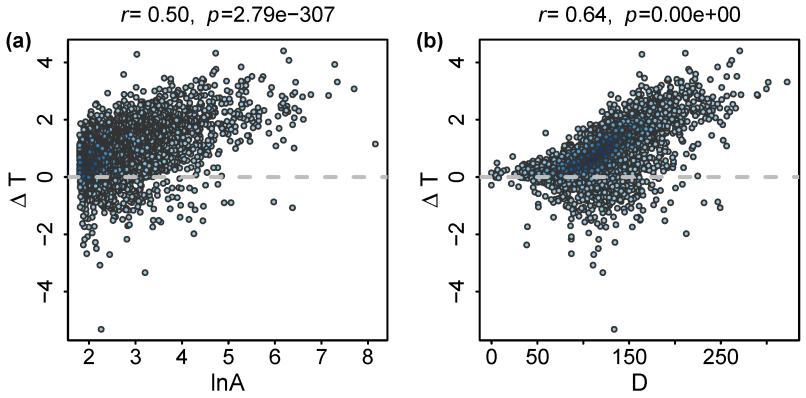

Figure S1: **Pearson correlation coefficient between (a) ΔT and $\ln A$, (b) ΔT and D**

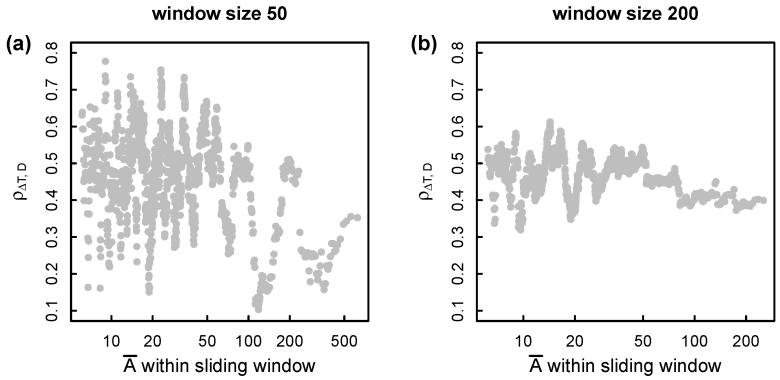

Figure S2: **Pearson correlation coefficient between the ΔT and D of the sample set selected by a sliding window, plotted against the average area A of the sample set.** The sample sets are selected using a window size (number of cities within each sample set) of 50 (panel **a**) and 200 (panel **b**) according to their ranking in area, so that cities within one sample set have a similar value of area A, the smaller the window size, the closer the area values.

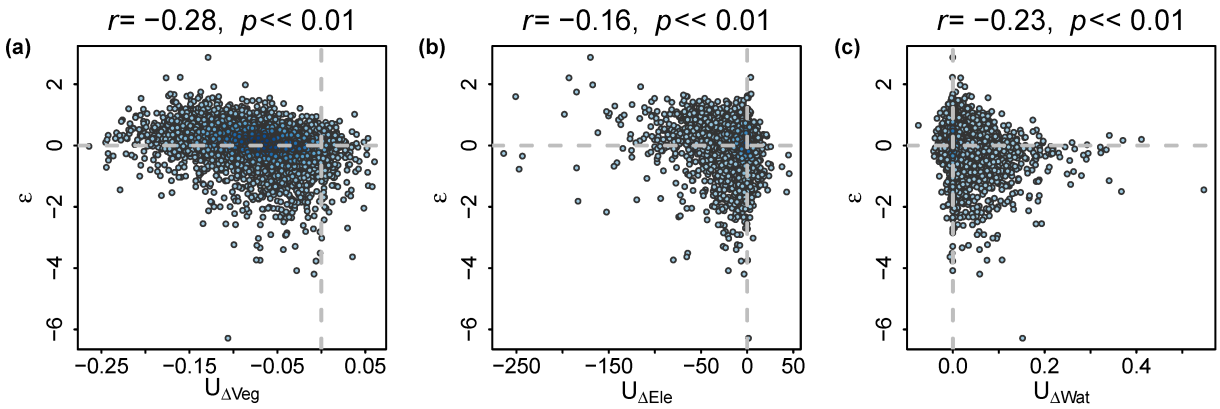

Figure S3: **Residuals from regression of Eq. (3) against $U_{\Delta Wat}$, $U_{\Delta Veg}$ and $U_{\Delta Ele}$.**

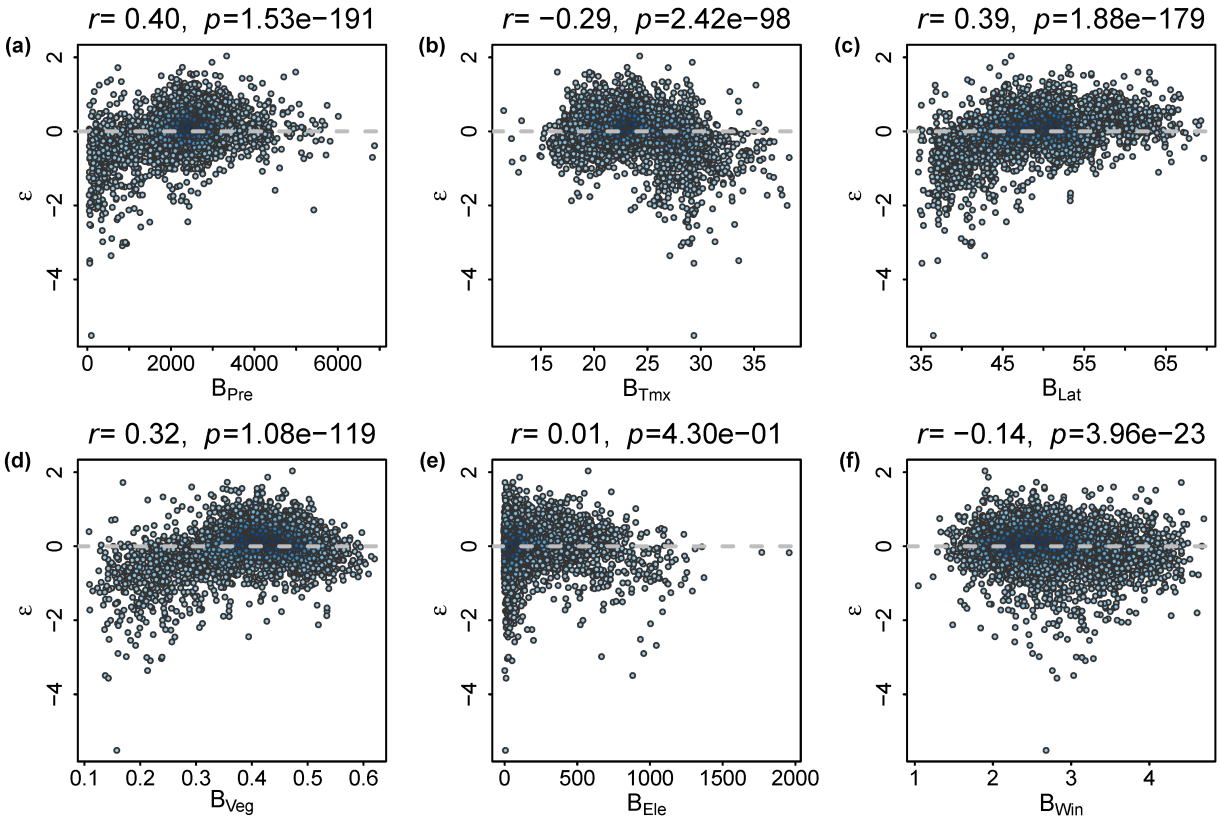

Figure S4: **Residuals from fitting of Eq. (4) against background biophysical factors.** (a) summer precipitation B_{Pre}. (b) summer mean maximum temperature B_{Tmx}. (c) latitude B_{Lat}. (d) summer EVI of boundary area B_{veg}. (e) elevation B_{Ele}. (f) summer 10m wind speed B_{Win}.

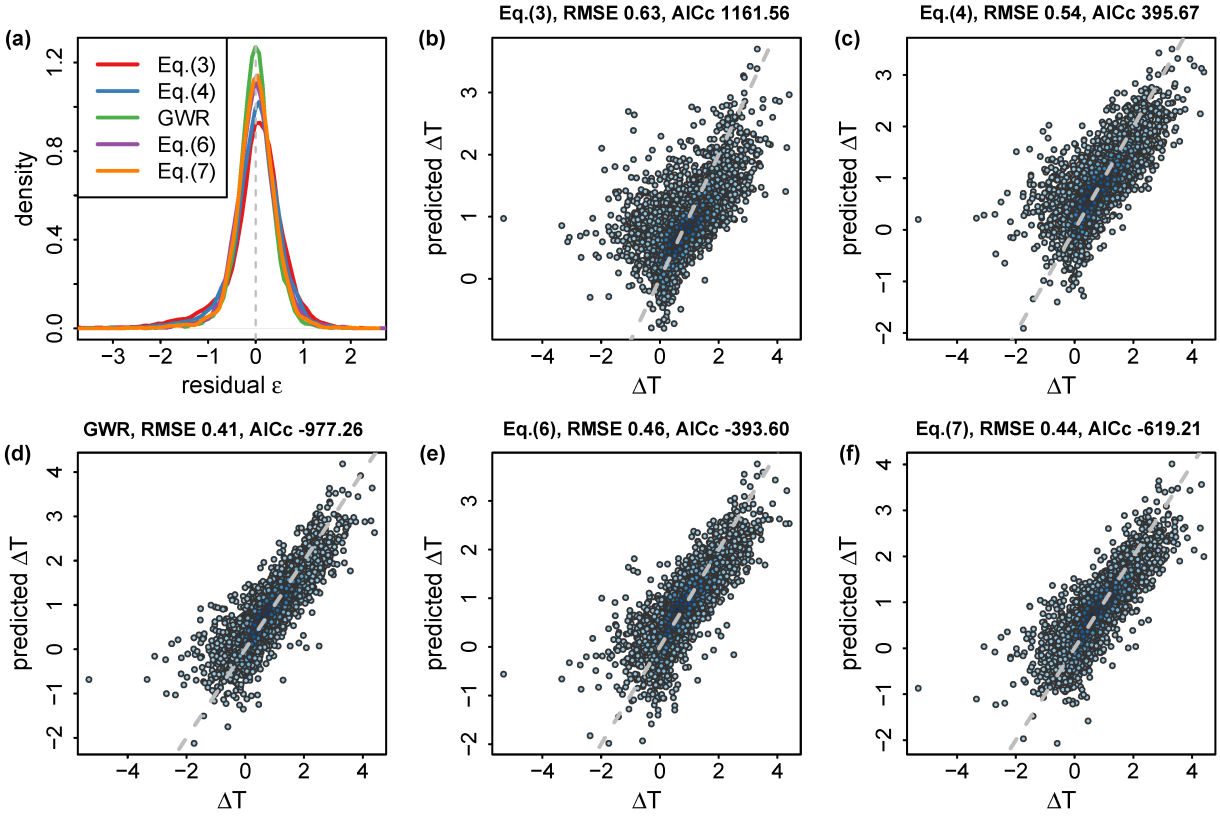

Figure S5: **Comparison of residuals from fitting of Eq. (3), Eq. (4), GWR, Eq. (6), Eq. (7).**

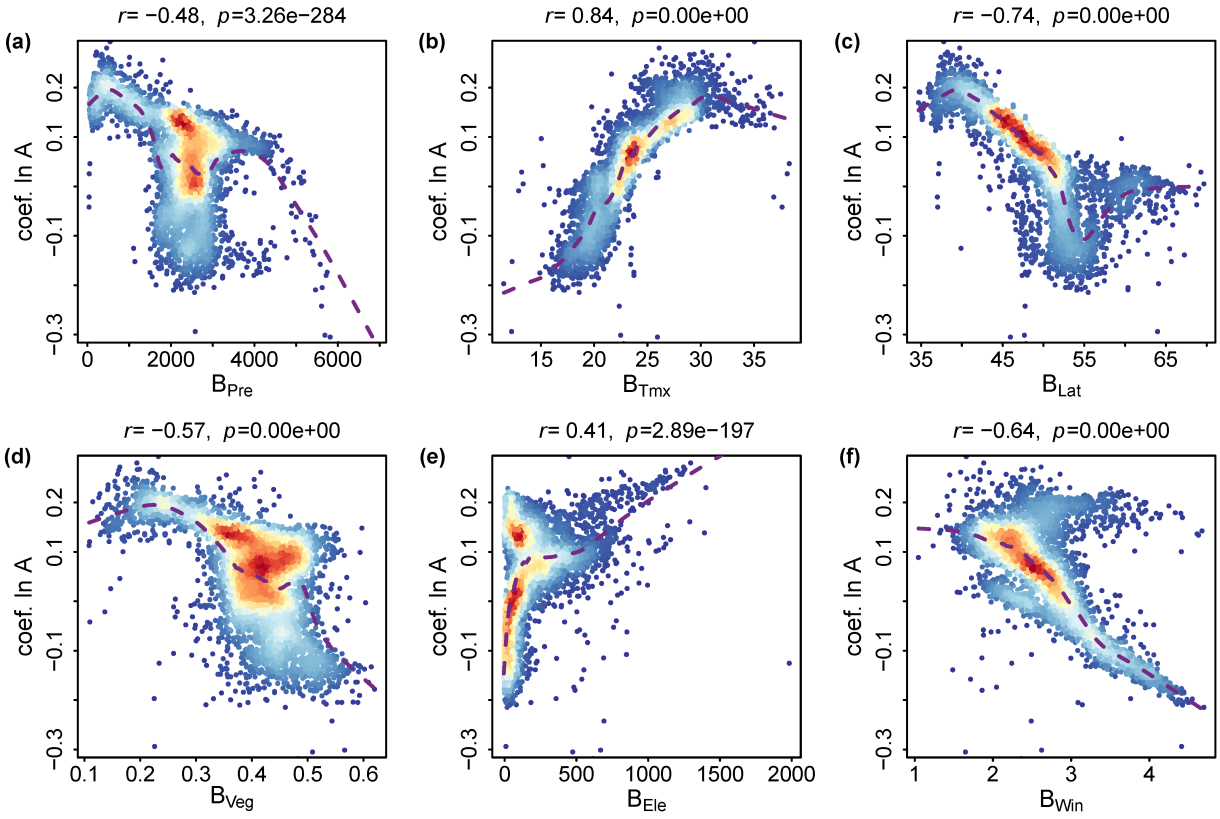

Figure S6: **Coefficient of** $\ln A$ **from GWR against the background biophysical factors.**

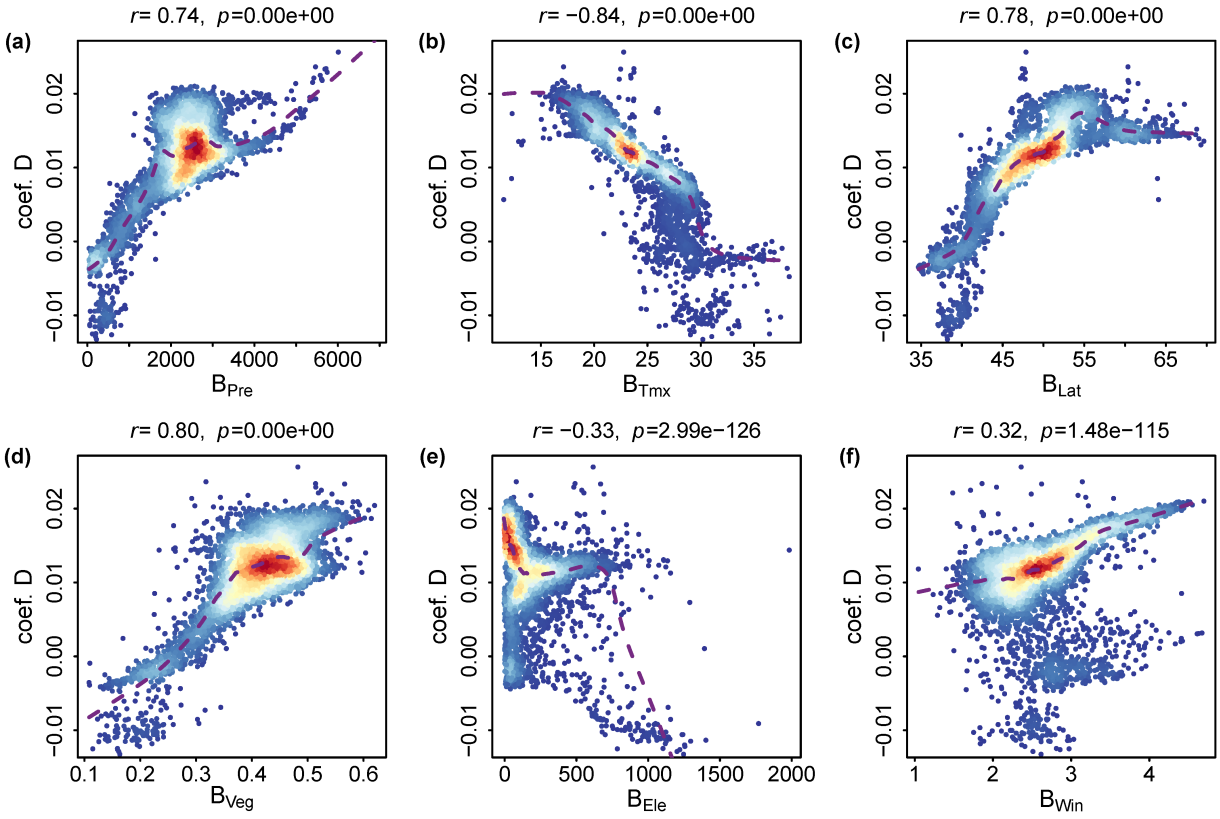

Figure S7: **Coefficient of D from GWR against the background biophysical factors.**

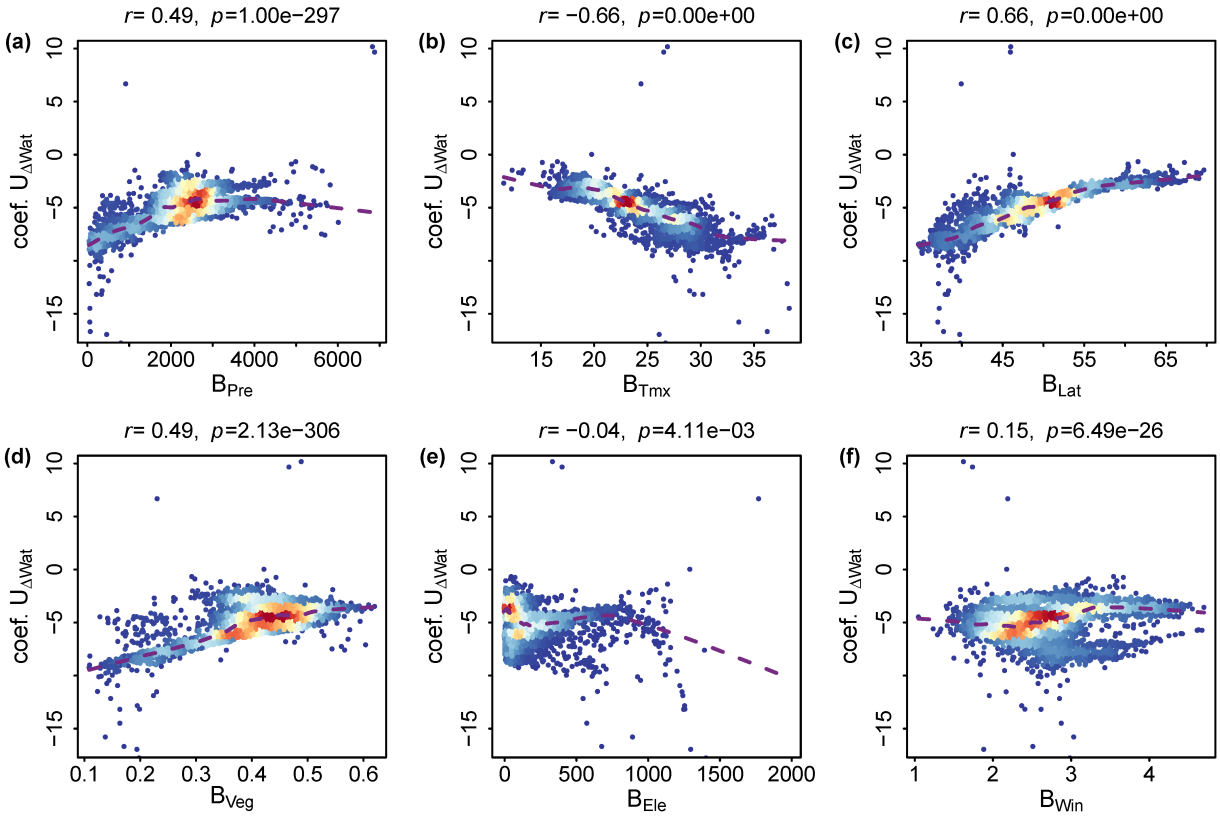

Figure S8: **Coefficient of $U_{\Delta Wat}$ from GWR against the background biophysical factors.**

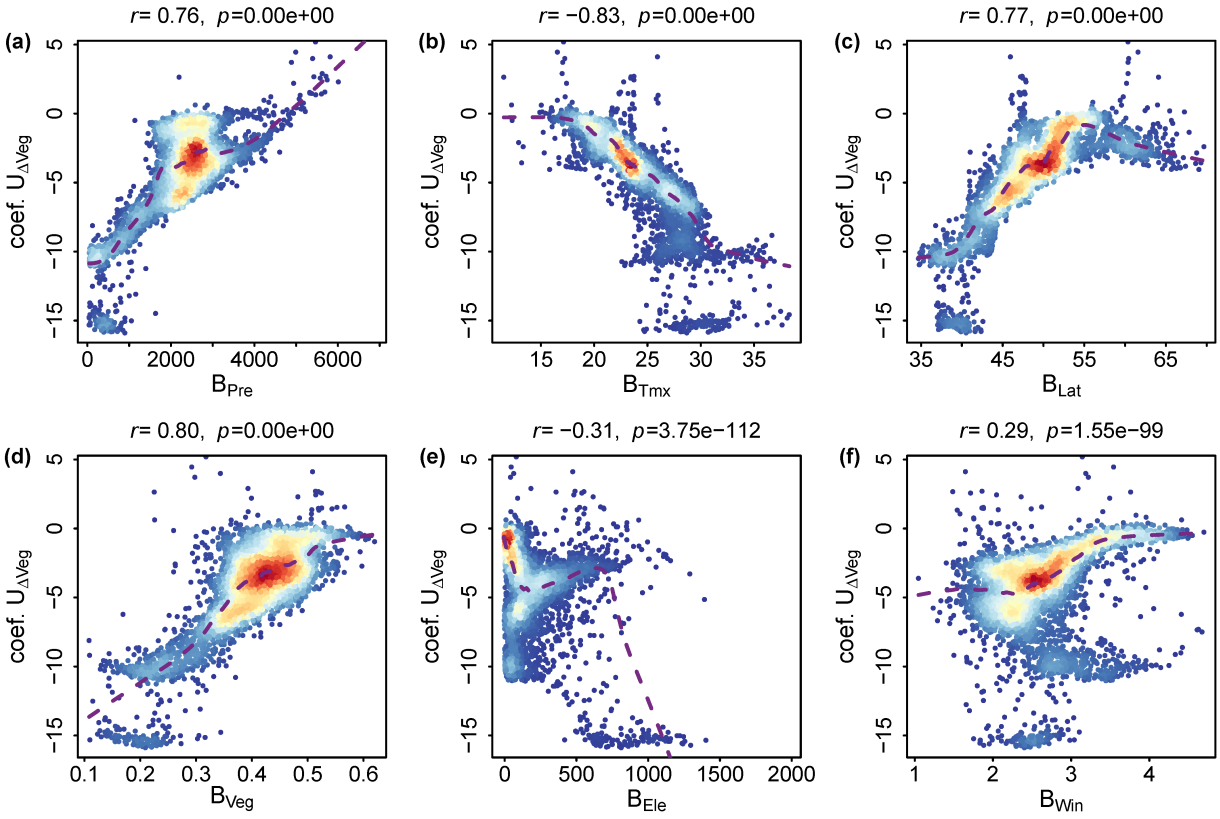

Figure S9: **Coefficient of $U_{\Delta Veg}$ from GWR against the background biophysical factors.**

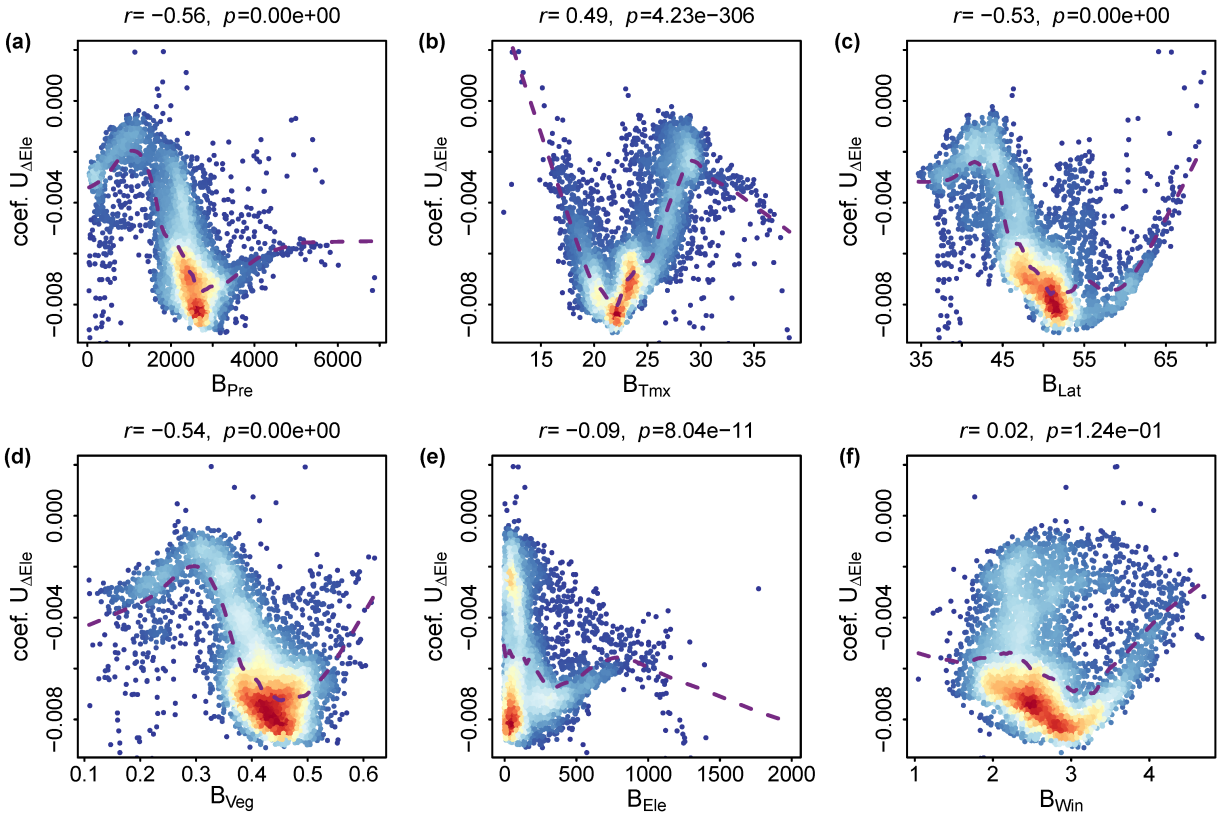

Figure S10: **Coefficient of $U_{\Delta Ele}$ from GWR against the background biophysical factors.**

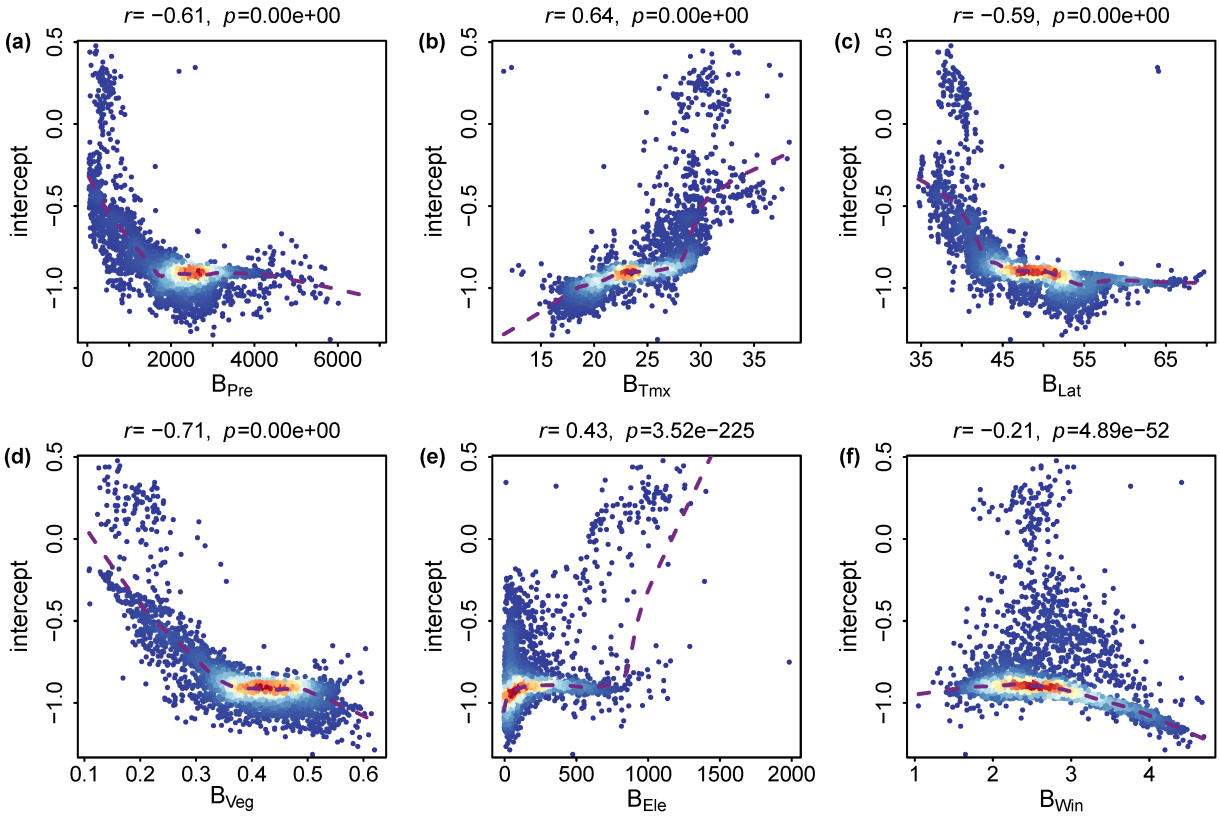

Figure S11: **Intercept from GWR against the background biophysical factors.**

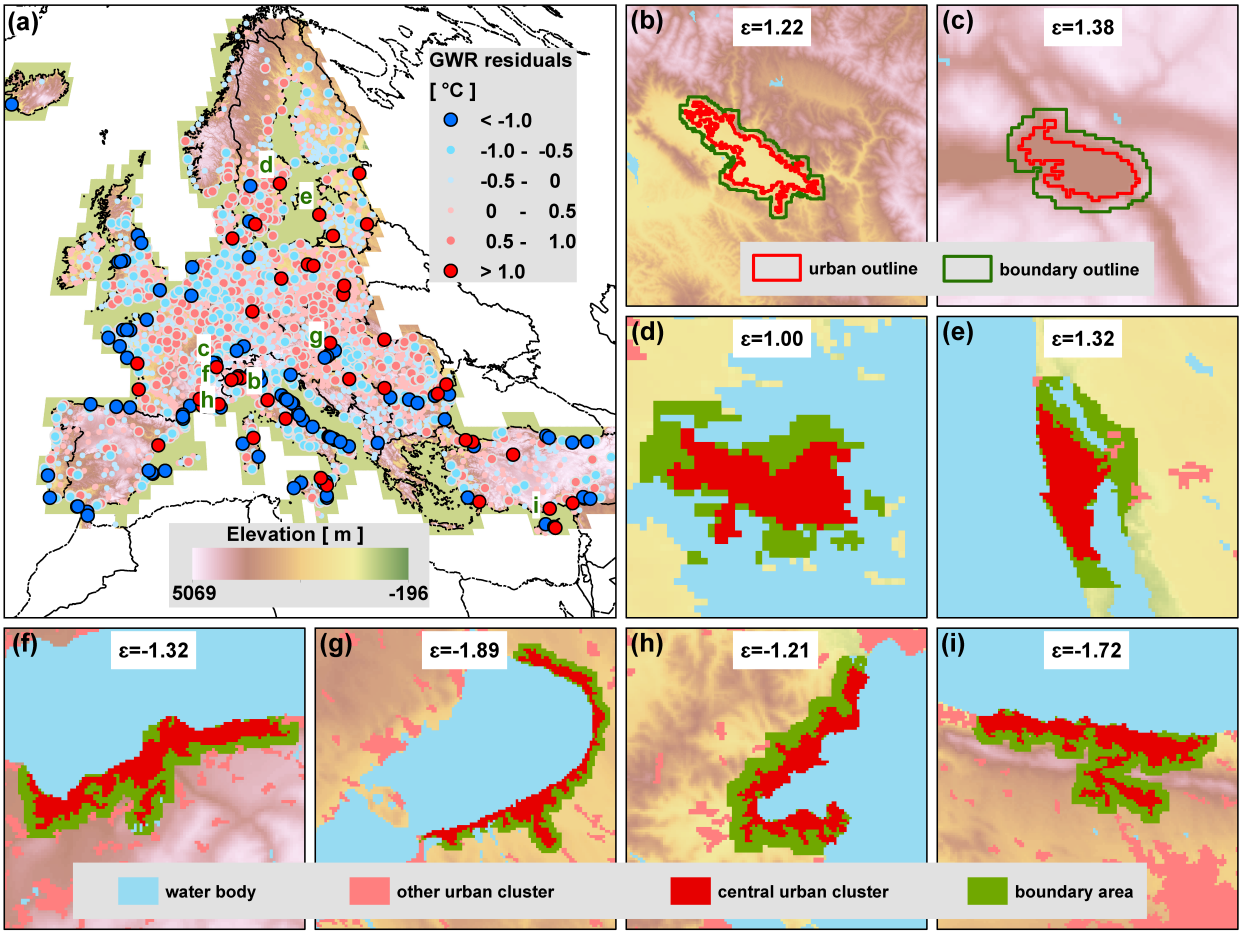

Figure S12: **Examples with large residuals (observed ΔT - model predicted ΔT) of the GWR model.** (a) the spatial distribution of the residuals overlapping on the elevation map. (b-e) examples of cities with very large positive residual (ϵ). (f-i) examples of cities with very large negative residual.

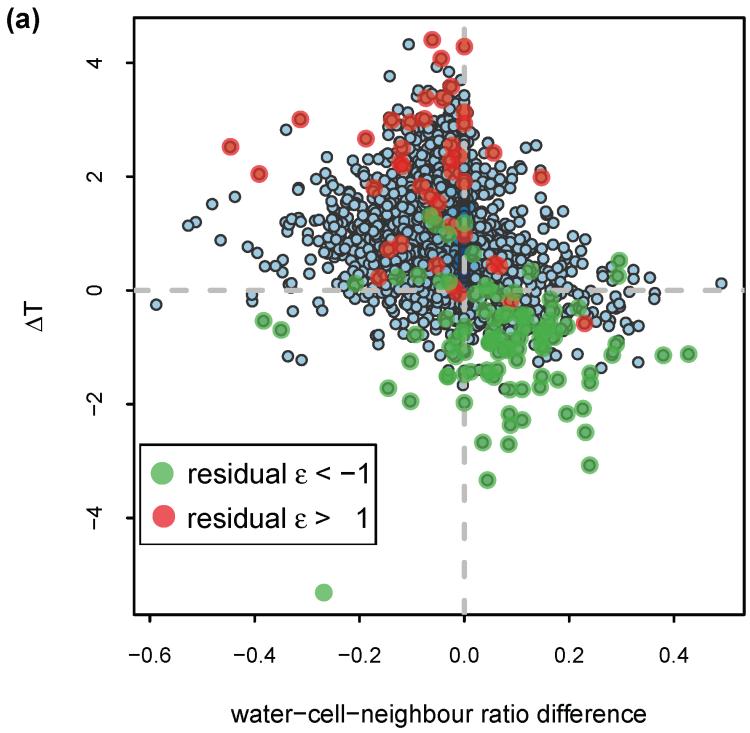

Figure S13: ΔT **plotted against the water-cell-neighbour ratio difference between urban area and boundary area.** The water-cell-neighbour ratio is calculated as number of neighbouring water body cells of a cluster divided by the number of cells of this area. For each city the water-cell-neighbour ratio is calculated for the urban cluster and its boundary area respectively, and then the difference between them is calculated (ratio of urban cluster minus ratio of boundary area). Points highlighted in red are the ones with residual from GWR larger than 1°C, which means they have much larger ΔT than the GWR model predicted. While the ones in green have residual smaller than -1°C.

Table S1: **Pearson correlation coefficient between all the used variables.**

	Δ_T	$\ln A$	D	$U_{\Delta Veg}$	$U_{\Delta Wat}$	$U_{\Delta Ele}$	B_{Pre}	B_{Tmx}	B_{Lat}	B_{Veg}	B_{Ele}	B_{Win}
Δ_T		0.50	0.64	−0.53	−0.26	−0.16	0.34	−0.32	0.28	0.42	−0.04	0.06
$\ln A$	0.50		0.74	−0.26	0.003	−0.21	−0.02	−0.04	0.02	0.02	−0.05	0.08
D	0.64	0.74		−0.50	−0.14	−0.05	−0.10	−0.07	0.01	−0.07	−0.13	0.26
$U_{\Delta Veg}$	−0.53	−0.26	−0.50		−0.15	0.12	−0.18	0.27	−0.12	−0.47	0.16	−0.24
$U_{\Delta Wat}$	−0.26	0.003	−0.14	−0.15		−0.13	−0.08	0.003	0.06	−0.09	−0.15	−0.002
$U_{\Delta Ele}$	−0.16	−0.21	−0.05	0.12	−0.13		−0.07	−0.07	0.16	−0.09	−0.35	0.21
B_{Pre}	0.34	−0.02	−0.10	−0.18	−0.08	−0.07		−0.53	0.55	0.73	0.06	−0.11
B_{Tmx}	−0.32	−0.04	−0.07	0.27	0.003	−0.07	−0.53		−0.84	−0.59	0.21	−0.46
B_{Lat}	0.28	0.02	0.01	−0.12	0.06	0.16	0.55	−0.84		0.48	−0.32	0.24
B_{Veg}	0.42	0.02	−0.07	−0.47	−0.09	−0.09	0.73	−0.59	0.48		−0.07	0.04
B_{Ele}	−0.04	−0.05	−0.13	0.16	−0.15	−0.35	0.06	0.21	−0.32	−0.07		−0.44
B_{Win}	0.06	0.08	0.26	−0.24	−0.002	0.21	−0.11	−0.46	0.24	0.04	−0.44	

Table S2: **Pearson correlation coefficient between the GWR coefficients and the background biophysical factors.**

	B_{Pre}	B_{Tmx}	B_{Lat}	B_{Veg}	B_{Ele}	B_{Win}
Intercept	-0.61	0.64	-0.59	-0.71	0.43	-0.21
Coef. D	0.74	-0.84	0.78	0.80	-0.33	0.32
Coef. $\ln A$	-0.48	0.84	-0.74	-0.57	0.41	-0.64
Coef. $U_{\Delta Wat}$	0.49	-0.66	0.66	0.49	-0.04	0.15
Coef. $U_{\Delta Veg}$	0.76	-0.83	0.77	0.80	-0.31	0.29
Coef. $U_{\Delta Ele}$	-0.56	0.49	-0.53	-0.54	-0.09	0.02

References

Brinckmann, Sven; Bissolli, P., 2016. Decreg/miklip gridded data of near-surface temperature (2m) and wind speed (10m) in europe for the period 2001-2010.version v002. doi:10.5676/DWD_CDC/DECREG0110v2.

Brinckmann, S., Krähenmann, S., Bissolli, P., 2015. High-resolution daily gridded datasets of air temperature and wind speed for europe. ESSDD 8, 649–702. doi:10.5194/essdd-8-649-2015.

Büttner, G., Kosztra, B., Maucha, G., Pataki, R., 2012. Implementation and achievements of CLC2006. Tech. Rep.. European Topic Centre Land Use and Spatial Information, Eur. Environ. Agency. Barcelona. URL: https://land.copernicus.eu/user-corner/technical-library/implementation-and-achievements-of-clc2006.

Buyantuyev, A., Wu, J., 2010. Urban heat islands and landscape heterogeneity: linking spatiotemporal variations in surface temperatures to land-cover and socioeconomic patterns. Landscape ecology 25, 17–33. doi:10.1007/s10980-009-9402-4.

Chen, C., Wang, L., Myneni, R.B., Li, D., 2020. Attribution of land-use/land-cover change induced surface temperature anomaly: How accurate is the first-order taylor series expansion? Journal of Geophysical Research: Biogeosciences 125, e2020JG005787. doi:10.1029/2020JG005787.

Chun, B., Guldmann, J.M., 2018. Impact of greening on the urban heat island: Seasonal variations and mitigation strategies. Computers, Environment and Urban Systems 71, 165–176. doi:10.1016/j.compenvurbsys.2018.05.006.

Dai, Z., Guldmann, J.M., Hu, Y., 2018. Spatial regression models of park and land-use impacts on the urban heat island in central beijing. Science of the total environment 626, 1136–1147. doi:10.1016/j.scitotenv.2018.01.165.

Deilami, K., Kamruzzaman, M., Liu, Y., 2018. Urban heat island effect: A systematic review of spatio-temporal factors, data, methods, and mitigation measures. International journal of applied earth observation and geoinformation 67, 30–42. doi:10.1016/j.jag.2017.12.009.

Demuzere, M., Bechtel, B., Mills, G., 2019. Global transferability of local climate zone models. Urban climate 27, 46–63. doi:10.1016/j.uclim.2019.01.005.

Didan, K., 2015. Mod13a3 modis/terra vegetation indices monthly l3 global 1km sin grid v006 (data set)

nasa eosdis land process. doi:10.5067/MODIS/MOD13Q1.006.

Du, H., Song, X., Jiang, H., Kan, Z., Wang, Z., Cai, Y., 2016. Research on the cooling island effects of water body: A case study of shanghai, china. Ecological indicators 67, 31–38. doi:10.1016/j.ecolind.2016.02.040.

Estrada, F., Botzen, W.W., Tol, R.S., 2017. A global economic assessment of city policies to reduce climate change impacts. Nature Climate Change 7, 403–406. doi:10.1038/nclimate3301.

Fluschnik, T., Kriewald, S., García Cantú Ros, A., Zhou, B., Reusser, D.E., Kropp, J.P., Rybski, D., 2016. The size distribution, scaling properties and spatial organization of urban clusters: a global and regional percolation perspective. ISPRS International Journal of Geo-Information 5, 110. doi:10.3390/ijgi5070110.

Fotheringham, A.S., Brunsdon, C., Charlton, M., 2003. Geographically weighted regression: the analysis of spatially varying relationships. John Wiley & Sons.

Gabriel, K.M., Endlicher, W.R., 2011. Urban and rural mortality rates during heat waves in berlin and brandenburg, germany. Environmental pollution 159, 2044–2050. doi:10.1016/j.envpol.2011.01.016.

Galletti, C.S., Li, X., Connors, J.P., 2019. Establishing the relationship between urban land-cover configuration and night time land-surface temperature using spatial regression. International Journal of Remote Sensing 40, 6752–6774. doi:10.1080/01431161.2019.1594432.

Geletič, J., Lehnert, M., Savić, S., Milošević, D., 2019. Inter-/intra-zonal seasonal variability of the surface urban heat island based on local climate zones in three central european cities. Building and Environment 156, 21–32. doi:10.1016/j.buildenv.2019.04.011.

Grimm, N.B., Faeth, S.H., Golubiewski, N.E., Redman, C.L., Wu, J., Bai, X., Briggs, J.M., 2008. Global change and the ecology of cities. science 319, 756–760. doi:10.1126/science.1150195.

Gudipudi, R., Rybski, D., Lüdeke, M.K., Zhou, B., Liu, Z., Kropp, J.P., 2019. The efficient, the intensive, and the productive: Insights from urban kaya scaling. Applied energy 236, 155–162. doi:10.1016/j.apenergy.2018.11.054.

Guo, A., Yang, J., Xiao, X., Xia, J., Jin, C., Li, X., 2020. Influences of urban spatial form on urban heat

island effects at the community level in china. Sustainable Cities and Society 53, 101972. doi:10.1016/j.scs.2019.101972.

He, B.J., 2018. Potentials of meteorological characteristics and synoptic conditions to mitigate urban heat island effects. Urban climate 24, 26–33.

Hooker, J., Duveiller, G., Cescatti, A., 2018. A global dataset of air temperature derived from satellite remote sensing and weather stations. Scientific data 5, 1–11. doi:10.1038/sdata.2018.246.

Jian, X., Olea, R.A., Yu, Y.S., 1996. Semivariogram modeling by weighted least squares. Computers & Geosciences 22, 387–397. doi:10.1016/0098-3004(95)00095-X.

Karger, D.N., Conrad, O., Böhner, J., Kawohl, T., Kreft, H., Soria-Auza, R.W., Zimmermann, N.E., Linder, H.P., Kessler, M., 2017. Climatologies at high resolution for the earth's land surface areas. Scientific data 4, 170122. doi:10.1038/sdata.2017.122.

Krummenauer, L., Prahl, B.F., Costa, L., Holsten, A., Walther, C., Kropp, J.P., 2019. Global drivers of minimum mortality temperatures in cities. Science of the total environment 695, 133560. doi:10.1016/j.scitotenv.2019.07.366.

Li, D., Liao, W., Rigden, A.J., Liu, X., Wang, D., Malyshev, S., Shevliakova, E., 2019. Urban heat island: Aerodynamics or imperviousness? Science Advances 5, eaau4299. doi:10.1126/sciadv.aau4299.

Li, H., Zhou, Y., Li, X., Meng, L., Wang, X., Wu, S., Sodoudi, S., 2018. A new method to quantify surface urban heat island intensity. Science of the total environment 624, 262–272. doi:10.1016/j.scitotenv.2017.11.360.

Li, J., Song, C., Cao, L., Zhu, F., Meng, X., Wu, J., 2011. Impacts of landscape structure on surface urban heat islands: A case study of shanghai, china. Remote sensing of environment 115, 3249–3263. doi:10.1016/j.rse.2011.07.008.

Li, S., Zhao, Z., Miaomiao, X., Wang, Y., 2010. Investigating spatial non-stationary and scale-dependent relationships between urban surface temperature and environmental factors using geographically weighted regression. Environmental Modelling & Software 25, 1789–1800. doi:10.1016/j.envsoft.2010.06.011.

Li, X., Zhou, Y., Asrar, G.R., Imhoff, M., Li, X., 2017. The surface urban heat island response to urban

expansion: A panel analysis for the conterminous united states. Science of the Total Environment 605, 426–435. doi:10.1016/j.scitotenv.2017.06.229.

Li, Y., Rybski, D., Kropp, J.P., 2021. Singularity cities. Environment and Planning B: Urban Analytics and City Science 48, 43–59. doi:10.1177/2399808319843534.

Li, Y., Schubert, S., Kropp, J.P., Rybski, D., 2020. On the influence of density and morphology on the urban heat island intensity. Nature communications 11, 1–9. doi:10.1038/s41467-020-16461-9.

Liang, Z., Wang, Y., Huang, J., Wei, F., Wu, S., Shen, J., Sun, F., Li, S., 2020. Seasonal and diurnal variations in the relationships between urban form and the urban heat island effect. Energies 13, 5909. doi:10.3390/en13225909.

Liu, H., Huang, B., Gao, S., Wang, J., Yang, C., Li, R., 2021a. Impacts of the evolving urban development on intra-urban surface thermal environment: Evidence from 323 chinese cities. Science of The Total Environment (onlinefirst). doi:10.1016/j.scitotenv.2020.144810.

Liu, H., Huang, B., Zhan, Q., Gao, S., Li, R., Fan, Z., 2021b. The influence of urban form on surface urban heat island and its planning implications: Evidence from 1288 urban clusters in china. Sustainable Cities and Society , 102987.

Liu, H., Zhan, Q., Gao, S., Yang, C., 2019. Seasonal variation of the spatially non-stationary association between land surface temperature and urban landscape. Remote Sensing 11, 1016. doi:10.3390/rs11091016.

Lu, B., Harris, P., Charlton, M., Brunsdon, C., 2014. The gwmodel r package: further topics for exploring spatial heterogeneity using geographically weighted models. Geo-spatial Information Science 17, 85–101. doi:10.1080/10095020.2014.917453.

Manoli, G., Fatichi, S., Bou-Zeid, E., Katul, G.G., 2020. Seasonal hysteresis of surface urban heat islands. Proceedings of the National Academy of Sciences 117, 7082–7089. doi:10.1073/pnas.1917554117.

Manoli, G., Fatichi, S., Schläpfer, M., Yu, K., Crowther, T.W., Meili, N., Burlando, P., Katul, G.G., Bou-Zeid, E., 2019. Magnitude of urban heat islands largely explained by climate and population. Nature 573, 55–60. doi:10.1038/s41586-019-1512-9.

Mathew, A., Khandelwal, S., Kaul, N., 2017. Investigating spatial and seasonal variations of urban heat

island effect over jaipur city and its relationship with vegetation, urbanization and elevation parameters. Sustainable Cities and Society 35, 157–177. doi:10.1016/j.scs.2017.07.013.

Morabito, M., Crisci, A., Guerri, G., Messeri, A., Congedo, L., Munafò, M., 2020. Surface urban heat islands in italian metropolitan cities: Tree cover and impervious surface influences. Science of The Total Environment 751, 142334. doi:10.1016/j.scitotenv.2020.142334.

Nakaya, T., Charlton, M., Lewis, P., Brunsdon, C., Yao, J., Fotheringham, S., 2014. Gwr4 windows application for geographically weighted regression modeling. Tempe: Geoda Center, Arizona State University .

Neter, J., Kutner, M.H., Nachtsheim, C.J., Wasserman, W., 1996. Applied linear statistical models. Irwin Chicago.

Ochola, E.M., Fakharizadehshirazi, E., Adimo, A.O., Mukundi, J.B., Wesonga, J.M., Sodoudi, S., 2020. Inter-local climate zone differentiation of land surface temperatures for management of urban heat in nairobi city, kenya. Urban Climate 31, 100540. doi:10.1016/j.uclim.2019.100540.

Oke, T.R., Mills, G., Voogt, J., 2017. Urban climates. Cambridge University Press.

Peng, S., Piao, S., Ciais, P., Friedlingstein, P., Ottle, C., Bréon, F.M., Nan, H., Zhou, L., Myneni, R.B., 2012. Surface urban heat island across 419 global big cities. Environmental science & technology 46, 696–703. doi:10.1021/es2030438.

Rozenfeld, H.D., Rybski, D., Andrade, J.S., Batty, M., Stanley, H.E., Makse, H.A., 2008. Laws of population growth. Proceedings of the National Academy of Sciences 105, 18702–18707. doi:10.1073/pnas.0807435105.

Rozenfeld, H.D., Rybski, D., Gabaix, X., Makse, H.A., 2011. The area and population of cities: New insights from a different perspective on cities. American Economic Review 101, 2205–25. doi:10.1257/aer.101.5.2205.

Simon, A., Fons, J., Milego, R., Georgi, B., 2010. Urban Morphological Zones version F2v0: Definition and procedural steps. Tech. Rep.. European Topic Centre Land Use and Spatial Information, Eur. Environ. Agency. Barcelona. URL: https://www.eea.europa.eu/data-and-maps/data/urban-morphological-zones-

2000-1.

Singh, P., Kikon, N., Verma, P., 2017. Impact of land use change and urbanization on urban heat island in lucknow city, central india. a remote sensing based estimate. Sustainable Cities and Society 32, 100–114. doi:10.1016/j.scs.2017.02.018.

Song, J., Chen, W., Zhang, J., Huang, K., Hou, B., Prishchepov, A.V., 2020. Effects of building density on land surface temperature in china: Spatial patterns and determinants. Landscape and Urban Planning 198, 103794. doi:10.1016/j.landurbplan.2020.103794.

Song, J., Du, S., Feng, X., Guo, L., 2014. The relationships between landscape compositions and land surface temperature: Quantifying their resolution sensitivity with spatial regression models. Landscape and Urban Planning 123, 145–157. doi:10.1016/j.landurbplan.2013.11.014.

Stewart, I.D., Oke, T.R., 2012. Local climate zones for urban temperature studies. Bulletin of the American Meteorological Society 93, 1879–1900. doi:10.1175/BAMS-D-11-00019.1.

Su, Y.F., Foody, G.M., Cheng, K.S., 2012. Spatial non-stationarity in the relationships between land cover and surface temperature in an urban heat island and its impacts on thermally sensitive populations. Landscape and Urban Planning 107, 172–180. doi:10.1016/j.landurbplan.2012.05.016.

Sultana, S., Satyanarayana, A., 2020. Assessment of urbanisation and urban heat island intensities using landsat imageries during 2000–2018 over a sub-tropical indian city. Sustainable Cities and Society 52, 101846. doi:10.1016/j.scs.2019.101846.

Szymanowski, M., Kryza, M., 2012. Local regression models for spatial interpolation of urban heat island—an example from wrocław, sw poland. Theoretical and applied climatology 108, 53–71. doi:10.1007/s00704-011-0517-6.

Tan, J., Zheng, Y., Tang, X., Guo, C., Li, L., Song, G., Zhen, X., Yuan, D., Kalkstein, A.J., Li, F., et al., 2010. The urban heat island and its impact on heat waves and human health in shanghai. International journal of biometeorology 54, 75–84. doi:10.1007/s00484-009-0256-x.

Wan, Z., Hook, S., Hulley, G., 2015. Mod11a2 modis/terra land surface temperature/emissivity 8-day l3 global 1km sin grid v006. NASA EOSDIS Land Processes DAAC 10. doi:10.5067/MODIS/MYD11A2.006.

Wang, J., Huang, B., Fu, D., Atkinson, P.M., 2015. Spatiotemporal variation in surface urban heat island intensity and associated determinants across major chinese cities. Remote Sensing 7, 3670–3689. doi:10.3390/rs70403670.

Wang, Y., Zhan, Q., Ouyang, W., 2019. How to quantify the relationship between spatial distribution of urban waterbodies and land surface temperature? Science of the Total Environment 671, 1–9. doi:10.1016/j.scitotenv.2019.03.377.

Yang, J., Wang, Y., Xiao, X., Jin, C., Xia, J.C., Li, X., 2019. Spatial differentiation of urban wind and thermal environment in different grid sizes. Urban Climate 28, 100458. doi:10.1016/j.uclim.2019.100458.

Yin, C., Yuan, M., Lu, Y., Huang, Y., Liu, Y., 2018. Effects of urban form on the urban heat island effect based on spatial regression model. Science of the Total Environment 634, 696–704. doi:10.1016/j.scitotenv.2018.03.350.

Yu, Z., Xu, S., Zhang, Y., Jørgensen, G., Vejre, H., 2018. Strong contributions of local background climate to the cooling effect of urban green vegetation. Scientific reports 8, 1–9. doi:10.1038/s41598-018-25296-w.

Zhang, P., Imhoff, M.L., Bounoua, L., Wolfe, R.E., 2012. Exploring the influence of impervious surface density and shape on urban heat islands in the northeast united states using modis and landsat. Canadian Journal of Remote Sensing 38, 441–451. doi:10.5589/m12-036.

Zhang, Y., Middel, A., Turner, B., 2019. Evaluating the effect of 3d urban form on neighborhood land surface temperature using google street view and geographically weighted regression. Landscape Ecology 34, 681–697. doi:10.1007/s10980-019-00794-y.

Zhao, L., Lee, X., Smith, R.B., Oleson, K., 2014. Strong contributions of local background climate to urban heat islands. Nature 511, 216–219. doi:10.1038/nature13462.

Zhou, B., Rybski, D., Kropp, J.P., 2013. On the statistics of urban heat island intensity. Geophysical research letters 40, 5486–5491. doi:10.1002/2013GL057320.

Zhou, B., Rybski, D., Kropp, J.P., 2017. The role of city size and urban form in the surface urban heat island. Scientific reports 7, 1–9. doi:10.1038/s41598-017-04242-2.

Zhou, D., Xiao, J., Bonafoni, S., Berger, C., Deilami, K., Zhou, Y., Frolking, S., Yao, R., Qiao, Z., Sobrino, J.A., 2019a. Satellite remote sensing of surface urban heat islands: progress, challenges, and perspectives. Remote Sensing 11, 48. doi:10.3390/rs11010048.

Zhou, D., Zhang, L., Li, D., Huang, D., Zhu, C., 2016. Climate–vegetation control on the diurnal and seasonal variations of surface urban heat islands in china. Environmental Research Letters 11, 074009. doi:10.1088/1748-9326/11/7/074009.

Zhou, D., Zhao, S., Liu, S., Zhang, L., Zhu, C., 2014. Surface urban heat island in china's 32 major cities: Spatial patterns and drivers. Remote Sensing of Environment 152, 51–61. doi:10.1016/j.rse.2014.05.017.

Zhou, W., Huang, G., Cadenasso, M.L., 2011. Does spatial configuration matter? understanding the effects of land cover pattern on land surface temperature in urban landscapes. Landscape and urban planning 102, 54–63. doi:10.1016/j.landurbplan.2011.03.009.

Zhou, Y., Li, D., Li, X., 2019b. The effects of surface heterogeneity scale on the flux imbalance under free convection. Journal of Geophysical Research: Atmospheres 124, 8424–8448. doi:10.1029/2018JD029550.